The role of pre-existing structures during rifting, continental breakup and transform system development, offshore West Greenland

Alexander L. Peace[1]

Ken J. W. McCaffrey[2]

Jonathan Imber[2]

Jeroen van Hunen[2]

Richard Hobbs[2]

Woody Wilson[3]

[1] Department of Earth Sciences, Memorial University of Newfoundland, St. John's, Newfoundland, Canada

[2] Department of Earth Sciences, Science Laboratories, Durham University, Durham, UK

[3] BP Exploration, Sunbury-on-Thames, Middlessex, UK

Abstract

Continental breakup between Greenland and North America produced the small oceanic basins of the Labrador Sea and Baffin Bay, which are connected via the Davis Strait, a region mostly comprised of continental crust. This study contributes to the debate regarding the role of pre-existing structures on rift development in this region using seismic reflection data from the Davis Strait data to produce a series of seismic surfaces, isochrons and a new offshore fault map from which three normal fault sets were identified as (i) NE-SW, (ii) NNW-SSE and (iii) NW-SE. These results were then integrated with plate reconstructions and onshore structural data allowing us to build a two-stage conceptual model for the offshore fault evolution in which basin formation was primarily controlled by rejuvenation of various types of pre-existing

structures. During the first phase of rifting between at least Chron 27 (ca. 62 Ma; Palaeocene), but potentially earlier, and Chron 24 (ca. 54 Ma; Eocene) faulting was primarily controlled by pre-existing structures with oblique normal reactivation of both the NE-SW and NW-SE structural sets in addition to possible normal reactivation of the NNW-SSE structural set. In the second rifting stage between Chron 24 (ca. 54 Ma; Eocene) and Chron 13 (ca. 35 Ma; Oligocene), the sinistral Ungava transform fault system developed due to the lateral offset between the Labrador Sea and Baffin Bay. This lateral offset was established in the first rift stage possibly due to the presence of the Nagssugtoqidian and Torngat terranes being less susceptible to rift propagation. Without the influence of pre-existing structures the manifestation of deformation cannot be easily explained during either of the rifting phases. Although basement control diminished into the post-rift, the syn-rift basins from both rift stages continued to influence the location of sedimentation possibly due to differential compaction effects. Variable lithospheric strength through the rifting cycle may provide an explanation for the observed diminishing role of basement structures through time.

Introduction

Understanding the mechanisms that govern continental breakup is crucial to further our understanding of the behaviour of the crust under extension (e.g. McKenzie, 1978; Lister *et al.*, 1991). Furthermore, such understanding is crucial in reducing the exploration risk at rifted continental margins by providing constraints for models and concepts used in exploration (e.g. Skogseid, 2001). One such group of interrelated mechanisms that may control various aspects of continental breakup is the influence of pre-existing geological structures (e.g. Theunissen *et al.*, 1996; Thomas *et al.*, 2006; Corti *et al.*, 2007; Gibson *et al.*, 2013; Manatschal *et al.*, 2015; Chenin *et al.*, 2015; Autin *et al.*, 2013; Petersen & Schiffer, 2016; Phillips *et al.*, 2016; Schiffer *et al.*, in press). Here, we investigate the role that pre-existing structures potentially played in continental breakup between Greenland and North America.

Pre-existing structures are defined as mechanical anisotropies in the pre-rift rocks that occur on a variety of scales from metamorphic mineral fabrics to major tectonic boundaries (Chattopadhyay & Chakra, 2013). Tectonic inheritance is the process by which pre-existing structure may influence a subsequent geological event (e.g.

Holdsworth *et al.*, 2001; Huerta & Harry, 2012). A complete geological cycle of tectonic inheritance has been proposed in which continental breakup occurs along the major weaknesses formed by older orogenic belts (Wilson, 1966; Ryan & Dewey, 1997; Petersen & Schiffer, 2016; Schiffer *et al.*, in press), although in certain instances orogenic activity may actually produce stronger lithosphere that is in fact harder to rift (Krabbendam, 2001). Previous work has shown that pre-existing structures can profoundly influence numerous aspects of the rifting process including; magmatism (Bureau *et al.*, 2013; Koopmann *et al.*, 2014), sedimentary basin geometry (Morley *et al.*, 2004), fault locations and timing (Korme *et al.*, 2004).

The rejuvenation of pre-existing crustal and lithospheric features during later tectonic events occurs via two related processes; reactivation and reworking (Dore *et al.*, 1997; Holdsworth *et al.*, 1997, 2001; Houseman & Molnar, 2001). Reactivation involves the rejuvenation of discrete structures (Butler *et al.*, 1997; Bellahsen *et al.*, 2006; Wu *et al.*, 2016), whereas reworking involves repeated focusing of metamorphism, deformation or magmatism on the same crustal or lithospheric volume (e.g. craton reactivation – Tappe *et al.*, 2007; repeated metamorphism – Manhica *et al.*, 2001; large-scale barriers to rift propagation – Koopmann *et al.*, 2014). However, both reactivation and reworking may represent the same processes operating at different scales and thus some ambiguity exists in distinguishing between these two processes in the literature (Holdsworth *et al.*, 2001). Of particular relevance to this study is the reactivation of discrete structures as a possible mechanism to produce normal faults that are not perpendicular to regional extension (e.g. Morley *et al.*, 2004; De Paola *et al.*, 2005) and the role of large-scale basement terranes during rifting (e.g. Krabbendam, 2001). In this study we consider the roles of both reactivation and reworking as end-member processes, both of which could have influenced the incomplete breakup of Greenland and North America in the Davis Strait.

Rifting between Greenland and Canada

The Labrador Sea and Baffin Bay (Fig. 1) formed due to divergent motion between Greenland and North America (e.g. Chalmers & Pulvertaft, 2001). According to Oakey & Chalmers (2012), breakup in this region occurred in three stages: (i) the Palaeocene separation between North America and Greenland which was still attached to Eurasia, (ii) the Eocene continued separation between Greenland and North America at the same time as separation between Eurasia and Greenland (Greenland moving as a separate plate) and (iii) since the Oligocene continued separation between Eurasia and Greenland with the latter attached to North America, i.e. the cessation of seafloor spreading to the west of Greenland (Fig. 2a).

Continental breakup between West Greenland and Eastern Canada resulted in oceanic spreading in the Labrador Sea and Baffin Bay but not the Davis Strait (Fig. 2a). The earliest rifting and the oldest, most extensive oceanic crust in the Labrador Sea – Baffin Bay system is found in the Southern Labrador Sea (e.g. Srivastava, 1978). Although lithospheric stretching in Baffin Bay is considered to have been sufficient to initiate seafloor spreading (Suckro *et al.*, 2012) the extent of oceanic crust in Baffin Bay is less than that of the Labrador Sea (e.g. Srivastava, 1978). The Davis Strait is a bathymetric high, primarily consisting of continental crust (Dalhoff *et al.*, 2006), linking the small oceanic basins of the Labrador Sea and Baffin Bay via the Ungava Fault Zone (UFZ) (Suckro *et al.*, 2013). The UFZ may represent a 'leaky transform' (Funck *et al.*, 2012) with small amounts of oceanic crust produced at pull-apart basin type settings but not full oceanic spreading (Srivastava, 1978).

The abundance and type of igneous rocks (Fig. 2a) also varies along the West Greenland Margin (e.g. Keen *et al.*, 2012). The margins of the southern Labrador Sea are non-volcanic (Chian *et al.*, 1995), however, they are volcanic in the northern Labrador Sea, Davis Strait (Keen *et al.*, 2012) and Baffin Bay (Suckro *et al.*, 2012). The Davis Strait is classified as a volcanic passive margin (Chalmers, 1997) due to the presence of volumetrically extensive igneous rocks (Storey *et al.*, 1998) and a 4- to 8-km-thick high velocity underplated layer (Funck *et al.*, 2007).

Basement terranes of west Greenland and north-eastern Canada

To determine the relationship, if any, between pre-existing geological structures and margin forming processes it is crucial to understand: (i) the sequence of events prior to rifting; (ii) the nature of the structural heterogeneities produced by previous events and (iii) the orientation of subsequent rifting with respect to pre-existing structures.

Nagssugtoqidian and Torngat Orogens

The Nagssugtoqidian Orogen (NO) is a belt of Paleoproterozoic deformation and metamorphism in West Greenland considered to have developed simultaneously with the Torngat Orogen (TO) in Labrador (Fig. 2b). The TO and NO belts are interpreted to have formed part of the same Paleoproterozoic passive margin prior to ocean closure and continental collision (Van Gool *et al*., 2002; Grocott & McCaffrey, 2017). A continental collision model of formation is preferred over earlier interpretations of an intracontinental strike-slip setting due to the presence of Paleoproterozoic calc-alkaline dykes that are attributed to a subduction zone-type setting (Korstgård *et al*., 1987). Reworked Achaean gneisses form a large majority of the NO (Van Gool *et al*., 2002). The NO contains multiple onshore structures that represent candidates for reactivation and reworking during rifting (Wilson *et al*., 2006).

The North Atlantic Craton and Nain Province

The North Atlantic Craton (NAC) is the Achaean terrane immediately to the south of the NO and north of the Ketilidian Mobile Belt (KMB) (Nutman & Collerson, 1991) (Fig. 2b, spanning the interval 3850–2550 Ma (Polat *et al*., 2014). The Nain Province (NP) of Labrador is considered to be the North American continuation of the NAC (St-Onge *et al*., 2009) (Fig. 2b). As with the NO, the NAC also contains multiple onshore structures that represent candidates for rejuvenation during rifting (Japsen *et al*., 2006).

Methodology and datasets

Two 2D seismic surveys were used in this study; the Spectrum West Greenland 2012 Repro and the BGR-77 survey alongside data from six exploration wells (Table 1 and Fig. 1). Interpretation and analysis of the data primarily utilized Schlumberger's Petrel, with further analysis conducted in ArcGIS, MATLAB and Generic Mapping Tools (GMT version 5). Seismic line spacing is variable from approximately 5–20 km in the south to 30–40 km in the north of the study area.

Table 1. Summary of exploration wells used in this study in the Davis Strait with the terminal depth (TD) in metres from the rotary table. Lithology at TD from Nøhr-Hansen (2003) and Rolle (1985)

Seismic interpretation

Twelve key seismic horizons, typically unconformities or high amplitude reflectors (Fig. 3), were traced across the data (Figs 4 and 5). The six exploration wells were then tied to the seismic data using the checkshots, with the seismic-well ties checked against the same ties reported in previous studies (Dalhoff *et al.*, 2003; Døssing, 2011). The seismic horizons were then dated using the nearest biostratigraphically dated samples in the wells (Rolle, 1985; Nøhr-Hansen, 2003; Piasecki, 2003; Rasmussen *et al.*, 2003). Where no material in the well was identified for a desired interval the position in the well was estimated by tracking seismic horizons that have been tied to surrounding wells and using the next oldest and youngest defined intervals as guidance. Some horizons were traced across the study area that could not be exactly tied to dated horizons in any well. This applied to six horizons in this study, two of which occur between the Late Lutetian and Middle Ypresian (the Middle Eocene 1–2 horizons), whereas the other three are between the basement horizon and the Late Thanetian (the Pre-Late Thanetian horizons 1–4). The horizons were then used to generate seismic surfaces, and then in turn used to generate isochrons. Isochrons were produced for the total sediment thickness (TST – seafloor to basement) and for intervals between 11 interpreted horizons between the seafloor and the basement within the polygon (Fig. 1).

Fault mapping and analysis

Faults that offset the top basement horizon were interpreted on individual seismic lines. These faults were then, where possible, linked between seismic lines based on orientation, size, style and proximity to one another and the free air gravity anomaly (FAA – Sandwell *et al.*, 2014) was used to guide fault interpretation. In total, 66 faults that offset the basement horizon were significant enough to tie between at least two seismic lines.

Polyline shapefiles depicting the faults were then created in ArcGIS, allowing an orientation analysis to be performed. Analysis of the fault population orientations was calculated for (i) the complete fault and (ii) for fault segments generated by splitting the polyline at the vertices prior to azimuth calculation. The second method provided a more realistic representation of fault orientation as many of the faults change azimuth along strike. Furthermore, a length scaling method was applied in order to incorporate the influence of structure size into our analysis of fault sets. The length scaling method used counts a particular fault (or fault segment) azimuth towards the corresponding azimuth bin total the same number of times as the fault length in km. For example in this analysis a structure of 1 km in length would be counted once, whereas a structure 100 km in length would be counted 100 times. This results in a scaled fault index rather than an absolute number of faults. Therefore, in order to fully characterize the distribution of faults into structural sets it was necessary to consider both the original (whole and split faults) in addition to the length scaled analysis.

Study limitations

Problems associated with the spatial distribution of the data are somewhat overcome by integration of the discrete seismic and well data with the continuous free air gravity and bathymetric data, whereas the effects of seismic line distribution was shown to be minimal by the grid thinning (Fig. 6). Another potential issue was utilizing biostratigraphic ages from the exploration wells (Nøhr-Hansen, 2003) as none of the wells penetrate deep into the syn-rift (Table 1). Also tracking seismic horizons over basement highs was problematic in small proximal basins without wells. During the fault mapping the method of only analysing faults capable of being tied between seismic lines could have induced spatial aliasing into our analysis. This is particularly relevant if the large faults follow a different trend to faults smaller than the seismic resolution. Finally, linking faults between 2D seismic lines may have resulting in miss-tied faults given that it cannot be indisputably determined using this type of data if faults are linked and if so what the nature of the link is, i.e. whether they are hard or soft-linked.

Results

Seismic horizons

Basement horizon

The rift-onset unconformity representing the basement horizon is a high amplitude reflector, between reflectors that display minimal organization and overlying reflections that are mostly characterized by conformable packages of sediments, some of which contain relatively high amplitude reflectors (Figs 4 and 5). Although little organization is displayed in the reflectors beneath this horizon (Fig. 5, line E), some high amplitude reflectors are present beneath which may represent intrusive rocks.

Pre-Late Thanetian Marker 4 (PLT 4)

This horizon is mostly represented by a high amplitude reflector or reflectors. PLT 4 is an unconformity, probably equivalent to the Middle Cretaceous Unconformity in Sørensen (2006). The reflectors that comprise PLT 4 are usually discontinuous but the horizon as a whole is easily recognized as the first high amplitude reflector above the basement horizon. The reflectors below are sometimes chaotic with individual horizons sometimes being difficult to distinguish and trace laterally, where they can be distinguished they are often truncated by PLT 4. The packages of sedimentary rocks beneath PLT 4 expand towards the footwalls of the faults that cut through PLT 4.

Pre-Late Thanetian Marker 3 (PLT 3)

PLT 3 lies conformably within the seismic sequence and is characterized by higher amplitude than the surrounding reflectors. The sequences between PLT 3 and 4 can been seen in some areas to expand away from basin bounding faults into the hanging wall sediments and in many locations to be crosscut by discontinuous, concave upwards, high amplitude reflectors most likely representing igneous intrusions (Fig. 4, line A), with a doming of the horizons above (forced folds – Magee *et al*., 2016). This horizon downlaps onto the PLT 4 and basement horizons (Fig. 4, line A; & Fig. 5, line E).

Pre-Late Thanetian Marker 2 (PLT 2)

The PLT 2 horizon lies conformably within the seismic sequence. The reflectivity of the surrounding sequences is variable from transparent to high amplitudes but PLT 2 always represents a higher amplitude horizon than the surrounding sequences.

Pre-Late Thanetian Marker 1 (PLT 1)

The PLT 1 marker is a conformable, slightly higher amplitude horizon within a relatively seismically transparent sequence. The package of reflections between PLT

2 and 1 thins from the centre of the study area to the north and south. On some profiles this horizon can be difficult to distinguish from the seismically transparent sequences in nearby proximity.

Late Thanetian (~54 Ma)

The Late Thanetian horizon is one of the key horizons interpreted as it is easily recognizable across the area and it represents an unconformity in the south of the area which potentially extends to the north. Sørensen (2006) recognized a Late Cretaceous unconformity which we interpret as erosion of sequences prior to this horizon. This horizon manifests in many areas as a high amplitude reflector, possibly from the Palaeogene flood basalts (e.g. Larsen *et al*., 1999). The packages from the four PLT horizons are truncated by the Late Thanetian horizon.

Middle Ypresian (~53 Ma)

This high amplitude horizon lies immediately above the unconformity at the top of a seismically low amplitude package of conformable sequences. The reflectors comprising this horizon are generally continuous (Fig. 4, lines B & C; Fig. 5, line D) except when this horizon is close in TWTT to the Late Thanetian horizon (Fig. 4, line A).

Middle Eocene Marker 2 (ME 2)

The ME 2 horizon is equivalent to the Middle Eocene unconformity (Sørensen, 2006). The nature of the reflectors constituting the ME 2 horizon varies across the study area, although its characteristics are sufficiently consistent for interpretation. ME 2 is located between a chaotic sediment package in which individual horizons are difficult to determine and the continuous sub-parallel overlying horizons. Where the surrounding packages are thinner in TWTT ME 2 is difficult to interpret, particularly in the south.

Middle Eocene Marker 1(ME 1)

ME 1 is a conformable, slightly higher amplitude horizon, within a low amplitude package. The reflectors that comprise this horizon (Fig. 4, line B & Fig. 5, line D) are usually discontinuous and stratigraphic relationships are sometimes difficult to interpret.

Late Lutetian (~41 Ma)

The late Lutetian horizon is a high amplitude reflector at the top of a low amplitude package, comprising sub-parallel reflectors, although in some areas it is chaotic and indistinct. The package of horizons between the Late Lutetian and the ME 1 expands northwards, containing many horizons that could be traced locally, and may belong to the Kangâmiut formation which is present in the north but not the south (Sørensen, 2006) (Fig. 3).

Base Early Pliocene (~5 Ma)

This horizon is equivalent to the Late Miocene unconformity (Sørensen, 2006) (Fig. 3), and is mostly characterized by medium to high amplitude reflectors. The sequences above downlap onto this horizon (Fig. 4, line D) and the stratigraphic successions above are typically sub-parallel, although sigmoidal packages are also present. The sequences above and below this horizon are discontinuous, particularly above basement highs in the south.

Late Pliocene (~3 Ma)

The Late Pliocene horizon is represented by conformable medium amplitude reflectors (Figs 4 and 5), which are mostly sub-parallel, although in the central and southern parts of the study area the packages beneath the Late Pliocene horizon are sigmoidal and discontinuous. Small disturbances to this horizon coincide with bathymetric lows, possibly representing disruption by fluid movements.

Seismic surfaces

The basement topography (Fig. 7A) is a high relief surface with lows below 7000 ms TWTT, whereas in other areas basement highs can be seen to be near the seafloor. In contrast the present bathymetric surface (Fig. 7M) is a low relief with essentially three key features: (i) a shallow water platform in the north and east; (ii) a deeper area occupying the area southwest and (iii) a channel incised to 3000 ms TWTT on the southern edge of the polygon.

Similarities exist between the basement (Fig. 7A) and the current bathymetric surfaces (Fig. 7M) including: (i) the elongate margin parallel basement high along the eastern edge of the polygon approximates the broad bathymetric high; (ii) some basement highs in the south are expressed as bathymetric highs and (iii) the elongate north-south basement low in the south coincides with the incised channel on the modern bathymetry. However, as expected the modern bathymetry more closely resembles the horizons interpreted within the post-rift (e.g. Fig. 7F–M), with the degree of similarity increasing as the post-rift progresses. Overall, through time the relief (horizon topography in TWTT) on the interpreted surfaces can be seen to progressively decrease.

Seismic isochrons

The isochrons are shown in Figs 8 and 9. In this section the terms ‘sedimentation’ and ‘deposition’ are used to refer to the time thickness infill recorded on the isochrons in TWTT (ms) that may also include volcanic rocks and does not make inferences about the rate of infill or amount of sediment flux.

Total sediment thickness

Total Sediment thickness (TST; Fig. 8a) was calculated between the seafloor and the basement horizon. Deep basins (>5000 ms TWTT) occur in the southern, central and northern parts of the study area. These deep basins form an approximately margin parallel chain with the major depocentres connected by thinner area of c. 3000 ms TWTT. Basins do occur outside of this chain across much of the south and in some isolated areas of the north but do not exceed c. 3000 ms TWTT and are spatially smaller (Fig. 8b).

Comparison of the TST isochron and the Bouger gravity anomaly (Fig. 8a & d) shows that the distribution of sedimentary basins alone does not explain the Bouger gravity anomaly. If the sedimentary basins are the sole contribution to the gravity anomalies it would be expected that gravity lows should coincide with deep basins and gravity highs with basement highs. Thus, because this relationship is not observed deeper structures must account for the variation in the anomalies. In the north of the area deep basins do coincide with gravity highs. However, it can be seen that the deep

NNE-SSW trending basin in the south has only a slightly lower gravity anomaly of c. 15–40 mGal compared with that of its surroundings of c. 40–80 mGal.

Large-scale temporal evolution: Basement to Late Thanetian and Late Thanetian to seafloor

Isochrons have not been produced for intervals that can be explicitly defined as syn-rift and post-rift, as it is unlikely that rifting ceased simultaneously across the study area, particularly given that multiple rifting events occurred (e.g. McGregor *et al.*, 2012). Instead, the Late Thanetian has been chosen to approximate the syn- to post-rift transition as it represents the first dated horizon and significantly different infill styles operate before and after (Fig. 9). Thus, comparison of pre- and post-Late Thanetian infill provides insights into the long-term differences between the early and late evolution of the study area.

The time thickness between the basement horizon and the Late Thanetian often represents the period of thickest sedimentary infill with over c. 3000 ms TWTT in many basins, particularly in the south (Fig. 8b). The largest depocentre is the NNE-SSW chain of basins in the south, but other significant depocentres are present. During this interval a distinct north-south disparity in basin aspect ratio is apparent, with the basins in the south tending to be more elongate than basins in the north.

The interval between the Late Thanetian and the modern seafloor (Fig. 8c) is dominated by a singular, elongate, margin parallel basin that for large parts is c. 4000 ms TWTT thick. Outside of the dominant basin preserved time thickness rarely exceeds c. 1500 ms TWTT.

Comparison between the pre- and post-Late Thanetian isochrons (Fig. 8b and c) shows that the large basins in the south received a greater amount of their time thickness infill during the earlier interval, whereas the large basin in the north received more during the later interval. Significant basins are located in the north of the study area during the latter interval but no significant time thickness infill is recorded in the south during the latter interval.

In summary, during the earlier interval deposition dominates the south in small discrete basins, whereas the later interval is dominated by more diffuse infill in the north. However, despite the large-scale difference observed between infill in the pre- and post-Late Thanetian intervals many areas that record lower time thickness infill during the earlier interval continue to receive lower amounts during the later interval. In addition, areas occupied by major basins during the earlier interval continue to record slightly higher infill than their surroundings in the later interval. The notable exception to this is in the southeast, where significant infill characterizes the earlier interval, whereas minimal infill is record in the later interval.

Onset of rifting to Late Thanetian

This is the interval between the basement and our first dated horizon (Late Thanetian) (Fig. 9A–E). Having considered the interval as a whole in the last section, here we focus on the detail shown by markers PLT 1-4 from oldest to youngest.

Between the basement horizon and the PLT marker 4 (Fig. 9A) many small depocentres are present across the study area. Some deposition occurred along the location of the major elongate basin(s) in the south of the study area where subsequent intervals also show significant infill.

Between the PLT marker 4 and PLT marker 3 (Fig. 9B) this major north-south basin in the south of the study area dominates deposition and the small depocentres which characterized the previous interval are less abundant. Some of the large depocentres from the previous interval, particularly in the central and northern parts of the study area, are now characterized by areas of lower sedimentation.

Between PLT Markers 2 and 3 (Fig. 9C), infill is characterized by diffuse deposition particularly in the northeast and southwest of the study area and deposition in the north-south elongate basin is lower than the previous two intervals.

The interval between PLT Markers 2 and 1 (Fig. 9D) records low sedimentation in a broadly similar distribution to the last interval. The largest depocentre in this interval is the area of diffuse sedimentation in the north where up to c. 500 ms TWTT of sediments are present.

Between PLT Marker 1 and the Late Thanetian horizon (Fig. 9E) the northern area is now one of minimal sedimentation, whereas infill accumulated in the small basins in the south with slightly thicker infill recorded at the location of the major southern basin that was identified during previous intervals.

Late Thanetian to Middle Ypresian

This interval (Fig. 9F) shows a different distribution of depocentres compared to previous intervals that resulted in distinct differences between infill patterns in the north and south. The area of thickest infill is a poorly defined basin in the north with lobes trending to the east and south away from the maximum thickness to the northwest. This depocentre appears to extend beyond our polygon with the greater infill to the west. The southern part of the study area during this interval is characterized by lower time thickness infill not exceeding c. 1000 ms and mostly less than c. 250 ms. Despite the southern area recording lower infill overall compared to the north, relatively more infill is recorded at the location of the major southern basin identified during previous intervals.

Middle Ypresian to Late Lutetian

The dominant basin between the Middle Ypresian and Mid Eocene Marker 2 (Fig. 9G) is coast parallel, displaying diffuse infill of c. 400 ms TWTT, with a step to the east in the south with the area of maximum infill located at the northern end of this basin. Between Mid Eocene marker 2 and Mid Eocene marker 1 (Fig. 9H) this basin shows a considerably reduced aspect ratio, with maximum thickness now located in the centre. A significant depocentre subsequently develops in the central northern part of the study area from Mid Eocene marker 1 to the Late Lutetian (Fig. 9I) containing c. 800 ms (TWTT) of infill. Outside of this major basin minimal sedimentation is recorded, particularly in the south.

Late Lutetian to early Pliocene

During this interval (Fig. 9J) significant depocentres were present in the north, whereas the central and southern areas record thin diffuse infill. Two small depocentres on the southern margin of the polygon are present, with the eastern most of these coinciding with the major elongate basin that dominated the southern part of the study area during the pre-Thanetian time intervals.

Early Pliocene to late Pliocene

During this interval (Fig. 9K) maximum sedimentation occurred in a basin in the centre of the polygon, where c. 400–800 ms (TWTT) is present. The significant basins in the north during the last interval are no longer present, with the north now recording reduced amounts of infill.

Late Pliocene to present

This interval (Fig. 9L) represents a period of significant deposition; particularly in the central and eastern areas. During this interval up to c. 1200 ms TWTT of infill was deposited in the centre of the main coast parallel basin.

North-south disparity

A north-south division is present on many of the isochrons and in the Bouguer gravity anomaly (Fig. 8d). Such a division is apparent on the Late Thanetian and the Middle Ypresian isochron (Fig. 9F) and on the Middle Eocene Marker 1 to the Late Lutetian isochron (Fig. 9I). In both of these intervals much greater amount of time thickness infill is recorded in the north than in the south. A north-south disparity is also observable in the earliest isochrons where southern basins have a much greater aspect ratio than northern basins. Bouguer gravity data also show north-south disparity with a strong positive anomaly across the south and a strong negative anomaly across much of the north (Fig. 8d).

Fault interpretation and mapping

This section describes the faults interpreted on seismic reflection profiles and the fault map.

Fault interpretation

All of the interpreted horizons are offset by normal faults, although fault offsets are larger (often >1000 ms) and faulting is more widespread within the lower (pre- PLT 2) successions. Normal fault offset is highly variable, although no particular area is dominated by much larger fault throws than elsewhere. Basement horizon offset of c. 1000 ms by normal faults is common with offsets up to c. 4000 ms being observed on the westward dipping normal fault bounding the large elongate N-S basin in the south. Dip generally decreases with depth on the large normal faults (offset >1000 ms) that offset the basement horizon.

Reverse faulting was also observed in proximity to the Ikermiut Fault Zone (IFZ – Gregersen & Skaarup, 2007; Chalmers & Pulvertaft, 2001). In the IFZ reverse faulting in close association with folding affects the successions prior to the Middle Ypresian Horizon (Fig. 5, Line D and Fig. 10, Line F). Thus, the age of this deformation is post-Middle Ypresian and pre-Middle Eocene 2. Folding was also observed in absence of reverse faulting but it more commonly occurs alongside reverse faults. Although several reverse faults were interpreted it was only possible to tie one of these across multiple (three) seismic lines (reverse fault 2 – Fig. 10).

Fault mapping

Fault mapping was conducted within the primary study area defined by the polygon (Fig. 1a) and further south along the West Greenland margin (Fig. 11). The extension to the south in which fault mapping was conducted was not included in the seismic horizon analysis due to the lack of well coverage, prohibiting a comparably reliable analysis from being conducted. Most faults have been mapped at depths of between 3000 and 6000 ms TWTT, however, a number of the larger faults reach depths of 7000 ms TWTT. The centre of the study area contains the highest density of shallow basement offsetting faults, which in some cases do not exceed depths of 4000 ms TWTT. The azimuth of the fault planes varies along strike on most of the faults and some also display variation in azimuth down dip on the fault plane. Thus, when analysing orientation the faults were divided into segments. Overall, it can be seen that the southern and central areas may contain a considerably greater density of normal faults. However, this could be due to sampling bias as a result of the denser seismic grid in the south.

The geographical distribution of faults mapped in our work is similar to the previous interpretation shown in Chalmers & Pulvertaft (2001) based on Chalmers, (1991) and Chalmers & Laursen, (1995), with the largest faults in our study corresponding with the majority of faults shown in Chalmers & Pulvertaft (2001). The principal difference between these interpretations is apparent in the south where the faults have now been mapped in greater detail due to the availability of more recent data. Several areas where no faults are shown on the Chalmers & Pulvertaft (2001) map have now been shown to have observable faults.

Analysis of fault strike is shown on rose diagrams in Fig. 12, with each fault analysed as a single polyline (Fig. 12a, b, e & f) and divided up at its vertices (Fig. 12c, d, f, g & h). In the non-length scaled results n=66 when the faults are not split at their vertices and n=152 when the faults are split at their vertices. The results of length scaling the fault population are shown on Fig. 12e–h. Based on orientation three fault sets were recognized in addition to the Ikermiut reverse faults. These are as follows: NE-SW (Fault Set 1), NNW-SSE (Fault Set 2) and NW-SE (Fault Set 3). The NNW-SSE oriented Fault Set 2 is more prominent when analysing the faults as segments divided on their vertices and when scaled by length. The longest faults and the faults with the largest (>3000 ms TWTT) offsets belong to fault sets 2 and 3. However, large faults do exist in fault set 1. The longest fault (c. 220 km long) belongs to fault set 3. The largest fault in fault set 1 occurs in the southeast of the interpretation polygon and is c. 60 km long, whereas the longest fault in fault set 2 is c. 120 km long.

Most of the brittle deformation documented in this study occurs prior to the Late Thanetian Horizon and in particular prior to the PLT 4 horizon (e.g. Fig. 4, lines a & c). However, it is evident that some deformation continues on rift-related structures into the Eocene successions, potentially due to differential sediment compaction between the syn-rift basins and highs. However, within the resolution of the data it was not possible to either relatively or absolutely constrain the timing of movement on each of the normal fault sets using the individual seismic lines, the surfaces or isochrons. This is evident on the earliest isochron from the Basement to the PLT 4 horizon whereby basins with orientations corresponding to all the fault sets identified can be seen to have formed (Fig. 9A). The reverse faults documented in the IFZ (Fig. 10) do not appear to extend beyond the Middle Ypresian.

Discussion

Through time the location and nature of the thickest infill in the area has changed from occurring in discrete fault bound basins, to more diffuse broad regions of infill

(Fig. 9). Here, the cause of this changing distribution is considered, alongside the relationship of the offshore structures and those previously published from onshore (Japsen *et al*., 2006; Wilson *et al*., 2006).

Comparison of on and offshore structures

The study area lies adjacent to both the NO and the NAC (Fig. 2b) but as the offshore continuation of the boundary between these terranes cannot be precisely located structures in both terranes are considered as candidates for rejuvenation. The north-south division displayed in many of the results of this study (e.g. fault density and basin size; Fig. 9F and I) may be linked to the location of the boundary between the Achaean NAC and the Proterozoic NO. Alternatively, the north-south division may be an artefact of the uneven distribution of the data, although the quality control grid thinning (described in the methodology) suggests that the influence of line density is minimal (Fig. 6), which indicates a geological explanation for this observation is plausible.

In addition to the boundary between the NO and the NAC (Fig. 2b) significant structural divisions within the NO may have also undergone rift-related reactivation, influencing the development of the offshore region. For example, comparison of the onshore geological map and cross section of Van Gool *et al*. (2002) (Section G) with an adjacent seismic line (Line G) from the offshore region (Fig. 13) demonstrates that the offshore continuation of the Nordre Strømfjord shear zone (NSSZ), Nordre Isortoq shear zone (NISZ) and Ikertôq thrust zone (ITZ) may correspond to distinct structures observable on this seismic line. In particular, on Line G it appears that the ITZ may correspond to the bounding fault of the basin shown on this line as the approximate continuation of the ITZ would be expected here, the dip direction of the basin bounding fault is similar and the reflection characteristics of the basement either side of this structure are what would be expected based on the onshore geology, i.e. the folded fabrics of the CNO and SNO display different internal reflectivity compared to within the ITZ (Wilson *et al*., 2006).

All three major fault sets identified in this work (Figs 11 and 12) correspond to structural systems identified onshore by Wilson *et al*. (2006) in the NO (Table 2). Purely based on orientation, without implying a causative link, the orientation of fault set 1 (NE-SW) in this study is similar to systems 1 (ENE-WSW) and 4 (NNE-SSW), fault set 2 (NNW-SSE) in this study is the same orientation as system 3 (NNW-SSE), whereas fault set 3 (NW-SE) in this study is of a similar orientation to systems 3 (NNW-SSE) and 5 (E-W to ESE-WNW) in Wilson *et al.* (2006). Given the close orientation of fault sets 2 and 3 in this study it cannot be determined to which of these fault sets system 3 in Wilson *et al.* (2006) may correspond to. Thus, system 3 in Wilson *et al.* (2006) is considered as a possible rejuvenation candidate for both fault sets 2 and 3. Wilson *et al.* (2006) suggested that system 1 has a similar trend to the dominant basement fabric in the NO, system 2 represents closely spaced faults often showing both sinistral and normal offset, system 3 is a closely spaced set of faults showing net dextral and normal offset of 20–40 m, system 4 structures are major subvertical sinistral strike-slip faults and fault zones and system 5 is a relatively localized set of dextral strike-slip structures.

The three major fault trends identified in this work also correspond to structural systems observed onshore in the Achaean NAC (Japsen *et al.*, 2006). Correlation based on orientation between the fault sets identified in this work and the outcrop analysis of Japsen *et al.* (2006), again without implying a causative link shows that fault set 1 (NE-SW) corresponds with the NE-SW trending deep gullies observed onshore; fault set 2 (NNW-SSE) is of a similar orientation to the N-S trending structure dipping moderately to the east, parallel to basement fabrics in the area; and fault set 3 (NW-SE) is the same orientation as the NW-SE trending joints and fractures which dip NE.

Comparison between on- and offshore structures demonstrates that there are certainly similarly oriented structures present both on and offshore. However, determining whether the structures are reactivated pre-existing structures or structures created during Mesozoic rifting requires examination of fault orientations with respect to rifting directions (e.g. Abdelmalak *et al.*, 2012). In the following sections fault orientations and the distribution of basin infill are considered in the context of a two-stage rifting model for the region (e.g. Wilson *et al.*, 2006; Abdelmalak *et al.*, 2012; Oakey & Chalmers, 2012).

Stage 1: rifting

This rifting stage (Fig. 14b) encompasses the oceanic magnetic anomalies from at least Chron 27 (ca. 62 Ma; Palaeocene), possibly earlier, to Chron 24 (ca. 54 Ma; Eocene) (Abdelmalak *et al*., 2012). However, extension in the region has been dated as early as the Late Triassic, with intense lithospheric stretching in the Early Cretaceous that produced dykes in West Greenland (Larsen *et al*., 2009) and their disputed minor equivalent in Labrador (Tappe *et al*., 2007; Peace *et al*., 2016). The isochrons documenting sediment distribution during this early rift interval are those prior to the Late Thanetian. Sediment deposition in this interval is focused into small isolated, fault bound basins that are in many places organized into ~N-S oriented chains (Fig. 9A and B).

The extension direction during this period was calculated by Abdelmalak *et al*. (2012) to be 069° ± 10 by inversion of fault-slip data using the inversion methodology described in Angelier (1990). The stress inversion conducted in West Greenland described by Abdelmalak *et al*. (2012) included 3300 measurements of fault-slip data from 60 measurement sites located in Palaeocene to Eocene basaltic formations. Most faults used in the Abdelmalak *et al*. (2012) inversion are relatively minor with throws not exceeding a few decimetres.

Of the three offshore fault populations identified by this study (Fig. 12) the closest to perpendicular to 069° ± 10, as would be expected when rifting a homogenous medium, is fault set 2 (NNW-SSE). Onshore in the NO domain Wilson *et al*. (2006) showed that a set of NNW-SSE faults are not the youngest structures and typically have a dextral strike-slip sense and that a N-S set of faults display normal and sinistral senses of movement. Whereas in the NAC domain, Japsen *et al*. (2006) documented a N-S structural trend as a prominent feature lying parallel to the basement fabric with a dextral sense. The slightly off-perpendicular orientation of these onshore structures with respect to rifting direction (Abdelmalak *et al*., 2012) could be due to the influence of a pre-existing structure set such as those identified onshore by Wilson *et al*. (2006) or it could be due to the error associated with the stress inversion (Abdelmalak *et al*., 2012) or the fault orientation analysis in this study.

Fault set 3 is the most dominant offshore structural trend in terms of the absolute number of faults and the size of the faults, some of which are the largest structures identified. Given the abundance and size of fault set 3, this fault set appears to represent the dominant manifestation of rift-related deformation. This is intriguing given the orientation of fault set 3 with respect to the extension direction (Abdelmalak *et al.*, 2012), which is difficult to reconcile without invoking the influence of pre-existing structures. The onshore studies have found multiple candidate structural sets that may have influenced the development of fault set 3. For example, onshore structures oriented NW-SE were identified in the NAC domain by Japsen *et al.* (2006). However, Japsen *et al.* (2006) were unable to determine any kinematic indicators on their NW-SE system. Furthermore, in the NO Wilson *et al.* (2006) identified a structural set oriented E-W to ESE-WSW which may also present a candidate structural set that influenced the development of fault set 3.

The NE-SW oriented fault set 1 has comparable abundance to fault set 2 but it is near parallel to the reconstructed extensional direction of 069° ± 10 (Abdelmalak *et al.*, 2012). Thus, it is difficult to reconcile these structures being involved in early rifting without invoking the reactivation of pre-existing structures in localizing deformation and a significant oblique slip component. Candidates for pre-existing structures related to fault set 1 are present onshore in the NAC domain where Japsen *et al.* (2006) observed a NE-SW structural set characterized by easily distinguishable yet poorly exposed deep, wide gullies. Furthermore, in the NO Wilson *et al.* (2006) documented an ENE-WSW fault set parallel to basement structures, displaying evidence for multiple phases and senses of movement. To summarize, fault set 1 would be unlikely to have developed without the influence of pre-existing structures.

Overall, during this interval fault location and orientation is primarily controlled by pre-existing structures (Fig. 14b) with fault set 1 (NE-SW) representing a highly oblique normal reactivation; fault set 2 (NNW-SSE) representing normal faults approximately orthogonal to the rifting direction that possibly, but not necessarily, always exploited pre-existing structures; and fault set 3 (NW-SE) representing oblique normal reactivation.

Our kinematic model for rift development in this interval is in broad agreement with the previously proposed reactivation model developed onshore that made predictions for the offshore by Wilson *et al*. (2006). Given that faulting is strongly controlled by pre-existing structures it follows that the location of depocentres during this interval, as depicted on the isochrons prior to the Late Thanetian, was also strongly controlled by pre-existing structures.

Stage 2: rifting and transform development

The second stage of extensional deformation (Fig. 14c) occurred between oceanic magnetic anomalies Chron 24 (ca. 54 Ma; Eocene) to Chron 13 (ca. 35 Ma; Oligocene), when Greenland moved north with respect to North America (e.g. Suckro *et al*., 2013), and regional extension has been calculated as ~N-S (178° ± 10 – Abdelmalak *et al*., 2012). The northward movement of Greenland caused sinistral deformation (Wilson *et al*., 2006) associated with the transform deformation on the UFZ (Kerr, 1967) including the areas of transpression such as the IFZ (Fig. 10). Deposition during this interval is minimal and chaotic in the south with poorly defined basins, whereas in the north a new basin is present (Fig. 9F). This may reflect deposition while a large-scale change in stress regime and rifting direction was taking place.

No faults in the study area were documented perpendicular to the proposed ~N-S extension direction (E-W) as would be expected under extension of a homogenous medium. It is therefore possible that deformation during this interval was influenced both by pre-rift structures and structures formed during stage 1 rifting. Although some deformation likely continued on fault sets 1, 2 and 3 the primary manifestation of deformation in this rifting stage is associated with the initiation and development of the UFZ. Our proposed model for this transform fault system is that offset between extension in Baffin Bay and the Labrador Sea was established during the first rifting stage, possibly due to the rift being unable to fully propagate through the NO and TO (Fig. 2b). Then in the second rifting stage when the extension vector changed to ~N-S (Abdelmalak *et al*., 2012) deformation was switched to transform system development. Thus, unlike in the first rifting interval where the rejuvenation pre-existing structures during rifting was through reactivation of discrete structures the role of pre-existing structures during the second rift stage influenced the large-scale manifestation of deformation through reworking as defined by (Holdsworth *et al*., 2001).

The nature of reactivation and the role of pre-existing structures through time

Overall, we propose that pre-existing structures of various origins, that possibly correspond to structures identified onshore (Japsen *et al*., 2006; Wilson *et al*., 2006), directly facilitated the subsequent localization of deformation during rifting which controlled the location and geometry of syn-rift deformation. We favour this over a scenario whereby pre-existing structures facilitated the development of localized stress fields which then interacted in the overburden to create structures oblique to the extension direction. The reason for this is that the structures mapped (Fig. 11) were observed to offset the pre-rift rocks (basement horizon) then not change strike considerably through the overlying material as would be expected with interacting stress fields.

Variable lithospheric strength through the rifting cycle may provide an explanation for the diminishing role of basement structures through time. In particular during stage 1 rifting where significant extensional deformation is inferred (Fig. 14b) it is possible that this lithospheric thinning resulted in an elevated geothermal gradient causing overall lithospheric weakening (Kusznir & Park, 1987). In such a situation the lithosphere may approach an Airy isostasy type situation whereby isostatic compensation would be extremely local, and may be accommodated by movement of discrete pre-existing structures. As rifting diminished and eventually ceased, cooling of the lithosphere would have resulted in an increase in lithospheric strength. Isostatic compensation of a stronger lithosphere favours broad regional flexure rather than localized faulting. Thus, the changing geothermal and strength profiles of the lithosphere through the rift cycle may provide an explanation for the reduced role of discrete, pre-existing structures through time, a possibility that should be investigated by future work in both the Davis Strait and elsewhere.

During the post-rift interval some expressions of rifting can be identified despite the influence of basement and rift-related structures diminishing. Firstly, the highs produced during rifting are often situated in similar locations to bathymetric highs (Fig. 7). The mechanism behind this phenomenon may be differential compaction, whereby less compaction occurs in the areas of minimal cover (Mesozoic highs) due to the presence of crystalline basement rocks. This mechanism may also explain why areas that were basins in the syn-rift continue to receive greater amounts of infill during the post-rift.

Petroleum systems implications

The small isolated basins depicted on the isochrons prior to PLT marker 3 (Fig. 9A–D) would provide a suitable location for the accumulation of organic matter in a spatially restricted environment that could lead to anoxic conditions indicative of preservation of organic matter. However, these small basins could make potential source rocks spatially limited and laterally variable. This is particularly important as the source rock interval offshore West Greenland is within the Cretaceous successions (Schenk, 2011). Finally, the thermal (e.g. Fjeldskaar *et al.*, 2008; Peace *et al.*, 2003) and structural (e.g. Magee *et al.*, 2017) implications of the widespread magmatism upon petroleum systems offshore West Greenland should also be considered during exploration.

Conclusions

Three fault systems were identified in the Davis Strait: (i) NE-SW, (ii) NNW-SSE and (iii) NW-SE, all of which correlate with structural trends identified onshore by previous work. During the first phase of rifting, faulting was primarily controlled by pre-existing structures with fault set 1 (NE-SW) representing oblique normal reactivation; fault set 2 (NNW-SSE) representing normal faults approximately orthogonal to extension possibly influenced by pre-existing structures and fault set 3 (NW-SE) representing oblique normal reactivation. In the second rifting stage, the sinistral UFZ transform system developed due to the lateral offset between the Labrador Sea and Baffin Bay. This lateral offset was established in the first rift stage possibly due to the presence of the NO-TO belt being unsusceptible to rift propagation. Without the influence of pre-existing structures the manifestation of deformation cannot be easily understood in the context of previously published rifting phases and directions.

The primary control on location and nature of rifting changed through time with basement anisotropy providing the main control on early faulting. The role of faulting and basement structures diminishes throughout the syn-rift and into the post-rift. However, pre-existing structures influenced certain aspects of the post-rift. The thermal regime and thus variations in lithospheric strength through the rift cycle may provide an explanation for the diminishing influence of pre-existing structures through time.

Finally, there is a distinct division between the north and south of the study area, with the syn-rift being dominated by deposition in the south, and the post-rift being dominated by deposition in the north. This long-lived division could reflect a significant pre-existing structure, potentially the offshore continuation of the NAC and NO boundary.

Acknowledgements

Funding for this research was primarily provided by Royal Dutch Shell in the form of a CeREES studentship at Durham University. The Durham University Center for Doctoral Training (CDT) in Energy and the Durham Energy Institute (DEI) are also thanked for their contribution towards the costs of this research. We would also like to thank Spectrum and BGR for providing access to the seismic data and Schlumberger for the Petrel software. Finally, we thank Dr. Craig Magee and two anonymous reviewers for their constructive reviews that significantly improved the quality of this manuscript.

Conflicts of interest

No conflict of interest declared.

References

Abdelmalak, M.M., Geoffroy, L., Angelier, J., Bonin, B., Callot, J.P., Gélard, J.P. & Aubourg, C. (2012) Stress fields acting during lithosphere breakup above a melting mantle: a case example in West Greenland. Tectonophysics, 581, 132–143.

Angelier, J. (1990) Inversion of field data in fault tectonics to obtain the regional stress-III. A new rapid direct inversion method by analytical means. Geophys. J. Int., 103(2), 363–376.

Autin, J., Bellahsen, N., Leroy, S., Husson, L., Beslier, M.O. & D'Acremont, E. (2013) The role of structural inheritance in oblique rifting: insights from analogue models and application to the Gulf of Aden. Tectonophysics, 607, 51–64.

Bellahsen, N., Fournier, M., d'Acremont, E., Leroy, S. & Daniel, J.M. (2006) Fault reactivation and rift localization: Northeastern Gulf of Aden margin. Tectonics, 25(1), 1–14.

Bureau, D., Mourgues, R., Cartwright, J., Foschi, M. & Abdelmalak, M.M. (2013) Characterisation of interactions between a pre-existing polygonal fault system and sandstone intrusions and the determination of paleo-stresses in the Faroe-Shetland basin. J. Struct. Geol., 46, 186–199.

Butler, R.W.H., Holdsworth, R.E. & Lloyd, G.E. (1997) The role of basement reactivation in continental deformation. J. Geol. Soc., 154(1), 69–71.

Chalmers, J.A. (1991) New evidence on the structure of the Labrador Sea/Greenland continental margin. J. Geol. Soc., 148(5), 899–908.

Chalmers, J.A. (1997) The continental margin off southern Greenland: along-strike transition from an amagmatic to a volcanic margin. J. Geol. Soc., 154(3), 571–576.

Chalmers, J.A. & Laursen, K.H. (1995) Labrador Sea: the extent of continental and oceanic crust and the timing of the onset of seafloor spreading. Mar. Pet. Geol., 12(2), 205–217.

Chalmers, J.A. & Pulvertaft, T.C.R. (2001) Development of the continental margins of the Labrador Sea: a review. Geol. Soc. London Spec. Publ., 187(1), 77–105.

Chattopadhyay, A. & Chakra, M. (2013) Influence of pre-existing pervasive fabrics on fault patterns during orthogonal and oblique rifting: an experimental approach. Mar. Pet. Geol., 39(1), 74–91.

Chenin, P., Manatschal, G., Lavier, L.L. & Erratt, D. (2015) Assessing the impact of orogenic inheritance on the architecture, timing and magmatic budget of the North Atlantic rift system: a mapping approach. J. Geol. Soc., 172, 711–720.

Chian, D., Keen, C., Reid, I. & Louden, K.E. (1995) Evolution of nonvolcanic rifted margins: new results from the conjugate margins of the Labrador Sea. Geology, 23(7), 589–592.

Corti, G., van Wijk, J., Cloetingh, S. & Morley, C.K. (2007) Tectonic inheritance and continental rift architecture: numerical and analogue models of the East African Rift system. Tectonics, 26(6), 1–13.

Dalhoff, F., Chalmers, J.A., Gregersen, U., Nøhr-Hansen, H., Rasmussen, J.A. & Sheldon, E. (2003) Mapping and facies analysis of Paleocene-Mid-Eocene seismic sequences, offshore southern West Greenland. Mar. Pet. Geol., 20(9), 935–986.

Dalhoff, F., Larsen, L.M., Ineson, J.R., Stouge, S., Bojesen-Koefoed, J.A., Lassen, S., Kuijpers, A., Rasmussen, J.A. & Nøhr-Hansen, H. (2006) Continental crust in the Davis Strait: new evidence from seabed sampling. Geol. Survey Denmark Greenland Bulletin, 10, 33–36.

De Paola, N., Holdsworth, R.E. & McCaffrey, K.J.W. (2005) The influence of lithology and pre-existing structures on reservoir-scale faulting patterns in transtensional rift zones. J. Geol. Soc., 162, 471–480.

Dore, A.G., Lundin, E.R., Fichler, C. & Olesen, O. (1997) Patterns of basement structure and reactivation along the NE Atlantic margin. J. Geol. Soc., 154(1), 85–92.

Døssing, A. (2011) Fylla Bank: structure and evolution of a normal-to-shear rifted margin in the northern Labrador Sea. Geophys. J. Int., 187(2), 655–676.

Fjeldskaar, W., Helset, H.M., Johansen, H., Grunnaleite, I. & Horstad, I. (2008) Thermal modelling of magmatic intrusions in the Gjallar Ridge, Norwegian Sea: implications for vitrinite reflectance and hydrocarbon maturation. Basin Res., 20, 143–159.

Funck, T., Jackson, H.R., Louden, K.E. & Klingelhofer, F. (2007) Seismic study of the transform-rifted margin in Davis Strait between Baffin Island (Canada) and

Greenland: what happens when a plume meets a transform. J. Geophys. Res.: Solid Earth, 112(4), B04402.

Funck, T., Gohl, K., Damm, V. & Heyde, I. (2012) Tectonic evolution of southern Baffin Bay and Davis Strait: results from a seismic refraction transect between Canada and Greenland. J. Geophys. Res.: Solid Earth, 117(4), B04107.

Gibson, G.M., Totterdell, J.M., White, L.T., Mitchell, C.H., Stacey, A.R., Morse, M.P. & Whitaker, A. (2013) Pre-existing basement structure and its influence on continental rifting and fracture zone development along Australia's southern rifted margin. J. Geol. Soc., 170(2), 365–377.

Gregersen, U. & Skaarup, N. (2007) A mid-Cretaceous prograding sedimentary complex in the Sisimiut Basin, offshore West Greenland-stratigraphy and hydrocarbon potential. Mar. Pet. Geol., 24(1), 15–28.

Grocott, J. & McCaffrey, K. (2017) Basin evolution and destruction in an early Proterozoic continental margin: the Rinkian fold-thrust Belt of Central West Greenland. J. Geol. Soc., https://doi.org/10.1144/jgs2016-109.

Holdsworth, R.E., Butler, C.A. & Roberts, A.M. (1997) The recognition of reactivation during continental deformation. J. Geol. Soc., 154(1), 73–78.

Holdsworth, R.E., Handa, M., Miller, J.A. & Buick, I.S. (2001) Continental reactivation and reworking: an introduction. Geol. Soc. London Spec. Publ., 184(1), 1–12.

Houseman, G. & Molnar, P. (2001) Mechanisms of lithospheric rejuvenation associated with continental orogeny. Geol. Soc. London Spec. Publ., 184, 13–38.

Huerta, A. & Harry, D.L. (2012) Wilson cycles, tectonic inheritance, and rifting of the North American Gulf of Mexico continental margin. Geosphere, 8(2), 374.

Japsen, P., Bonow, J.M., Peulvast, J.-P. & Wilson, R.W. (2006) Uplift, erosion and fault reactivation in southern West Greenland. GEUS Field Reports, 63.

Keen, C.E., Dickie, K. & Dehler, S.A. (2012) The volcanic margins of the northern Labrador Sea: insights to the rifting process. Tectonics, 31(1), 1–13.

Kerr, J.W. (1967) A submerged continental remnant beneath the Labrador Sea. Earth Planet. Sci. Lett., 2(4), 283–289.

Kerr, A., Hall, J., Wardle, R.J., Gower, C.F. & Ryan, B. (1997) New reflections on the structure and evolution of the Makkovikian – Ketilidian Orogen in Labrador and southern Greenland. Tectonics, 16(6), 942–965.

Koopmann, H., Brune, S., Franke, D. & Breuer, S. (2014) Linking rift propagation barriers to excess magmatism at volcanic rifted margins. Geology, 42(12), 1071–1074.

Korme, T., Acocella, V. & Abebe, B. (2004) The role of pre-existing structures in the origin, propagation and architecture of faults in the main Ethiopian rift. Gondwana Res., 7(2), 467–479.

Korstgård, J., Ryan, B. & Wardle, R. (1987) The boundary between Proterozoic and Archaean crustal blocks in central West Greenland and northern Labrador. Geol. Soc. London Spec. Publ., 27(1), 247–259.

Krabbendam, M. (2001) When the Wilson Cycle breaks down: how orogens can produce strong lithosphere and inhibit their future reworking. Geol. Soc. London Spec. Publ., 184(1), 57–75.

Kusznir, N.J. & Park, R.G. (1987) The extensional strength of the continental lithosphere: its dependence on geothermal gradient, and crustal composition and thickness. Geol. Soc. London Spec. Publ., 28(1), 35–52.

Larsen, H.C. & Saunders, A.D. (1998) Tectonism and volcanism at the southeast Greenland rifted margin: a record of plume impact and later continental rupture.

Proceedings of the Ocean Drilling Program, Scientific Results, 152, https://doi.org/10.2973/odp.proc.sr.152.1998.

Larsen, L.M., Rex, D.C., Watt, W.S. & Guise, P.G. (1999) 40Ar–39Ar dating of alkali basaltic dykes along the south-west coast of Greenland: cretaceous and Tertiary igneous activity along the eastern margin of the Labrador Sea. Geol. Greenland Survey Bulletin, 184, 19–29.

Larsen, L.M., Heaman, L.M., Creaser, R.A., Duncan, R.A., Frei, R. & Hutchison, M. (2009) Tectonomagmatic events during stretching and basin formation in the Labrador Sea and the Davis Strait: evidence from age and composition of Mesozoic to Palaeogene dyke swarms in West Greenland. J. Geol. Soc., 166(6), 999–1012.

Lister, G.S., Etheridge, M.A. & Symonds, P.A. (1991) Detachment models for the formation of passive continental margins. Tectonics, 10(5), 1038–1064.

Magee, C., Muirhead, J.D., Karvelas, A., Holford, S.P., Jackson, C.A.L., Bastow, I.D., Schofield, N., Stevenson, C.T.E., McLean, C., McCarthy, W. & Shtukert, O. (2016) Lateral magma flow in mafic sill complexes. Geosphere, 12(3), GES01256.

Magee, C., Jackson, C.A.-L., Hardman, J.P. & Reeve, M.T. (2017) Decoding sill emplacement and forced fold growth in the Exmouth Sub-basin, offshore northwest Australia: Implications for hydrocarbon exploration. Interpretation, 5(3), SK11–SK22.

Manatschal, G., Lavier, L. & Chenin, P. (2015) The role of inheritance in structuring hyperextended rift systems: some considerations based on observations and numerical modeling. Gondwana Res., 27(1), 140–164.

Manhica, A.D.S.T., Grantham, G.H., Armstrong, R.A., Guise, P.G. & Kruger, F.J. (2001) Polyphase deformation and metamorphism at the Kalahari Craton — Mozambique Belt boundary. Geol. Soc. London Spec. Publ., 184(1), 303–322.

McGregor, E.D., Nielsen, S.B., Stephenson, R.A., Clausen, O.R., Petersen, K.D. & Macdonald, D.I.M. (2012) Evolution of the west Greenland margin: offshore thermostratigraphic data and modelling. J. Geol. Soc., 169(5), 515–530.

McKenzie, D. (1978) Some remarks on the development of sedimentary basins. Earth Planet. Sci. Lett., 40(1), 25–32.

Morley, C.K., Haranya, C., Phoosongsee, W., Pongwapee, S., Kornsawan, A. & Wonganan, N. (2004) Activation of rift oblique and rift parallel pre-existing fabrics during extension and their effect on deformation style: examples from the rifts of Thailand. J. Struct. Geol., 26(10), 1803–1829.

Nøhr-Hansen, H. (2003) Dinoflagellate cyst stratigraphy of the Palaeogene strata from the Hellefisk-1, Ikermiut-1, Kangâmiut-1, Nukik-1, Nukik-2 and Qulleq-1 wells, offshore West Greenland. Mar. Pet. Geol., 20(9), 987–1016.

Nutman, A.P. & Collerson, K.D. (1991) Very early Archean crustal-accretion complexes preserved in the North Atlantic craton. Geology, 19(8), 791–794.

Oakey, G.N. & Chalmers, J. A. (2012) A new model for the Paleogene motion of Greenland relative to North America : plate reconstructions of the Davis Strait and Nares Strait regions between Canada and Greenland. J. Geophys. Res.: Solid Earth, 117 (B10), 1–28.

Peace, A., McCaffrey, K.J.W., Imber, J., Phethean, J., Nowell, G., Gerdes, K. & Dempsey, E. (2016) An evaluation of Mesozoic rift-related magmatism on the margins of the Labrador Sea: implications for rifting and passive margin asymmetry. Geosphere, 12(6), 1701–1724.

Peace, A., McCaffrey, K., Imber, J., Hobbs, R., van Hunen, J. & Gerdes, K. (2017) Quantifying the influence of sill intrusion on the thermal evolution of organic-rich sedimentary rocks in nonvolcanic passive margins: an example from ODP 210-1276, offshore Newfoundland, Canada. Basin Res., 29(3), 249–265.

Petersen, K.D. & Schiffer, C. (2016) Wilson cycle passive margins: control of orogenic inheritance on continental breakup. Gondwana Res., https://doi.org/10.1016/j.gr.2016.06.012.

Phillips, T.B., Jackson, C.A.-L., Bell, R.E., Duffy, O.B. & Fossen, H. (2016) Reactivation of intrabasement structures during rifting: a case study from offshore southern Norway. J. Struct. Geol., 91, 54–73.

Piasecki, S. (2003) Neogene dinoflagellate cysts from Davis Strait, offshore West Greenland. Mar. Pet. Geol., 20(9), 1075–1088.

Polat, A., Wang, L. & Appel, P.W.U. (2014) A review of structural patterns and melting processes in the Archean craton of West Greenland: evidence for crustal growth at convergent plate margins as opposed to non-uniformitarian models. Tectonophysics, 662, 67–94.

Rasmussen, J.A., Nøhr-Hansen, H. & Sheldon, E. (2003) Palaeoecology and palaeoenvironments of the lower palaeogene succession, offshore West Greenland. Mar. Pet. Geol., 20(9), 1043–1073.

Rolle, F. (1985) Late Cretaceous – Tertiary sediments offshore central West Greenland: Lithostratigraphy, sedimentary evoluation, and petroleum potential. Can. J. Earth Sci., 22(7), 1001–1029.

Ryan, P.D. & Dewey, J.F. (1997) Continental eclogites and the Wilson Cycle. J. Geol. Soc., 154(3), 437–442.

Sandwell, D.T., Müller, R.D., Smith, W.H.F., Garcia, E. & Francis, R. (2014) New global marine gravity model from CryoSat-2 and Jason-1 reveals buried tectonic structure. Science, 346(6205), 65–67.

Schenk, C.J. (2011) Chapter 41 geology and petroleum potential of the West Greenland-East Canada Province. Arctic Petrol. Geol., 35 (1), 627–645.

Schiffer, C., Peace, A., Phethean, J., Gernigon, L., McCaffrey, K.J.W., Petersen, K.D. & Foulger, G.R., (in press), The Jan Mayen Microplate complex and the Wilson Cycle: in tectonic evolution: 50 Years of the Wilson Cycle concept. Geol. Soc. London Spec. Publ.

Skogseid, J. (2001) Volcanic margins: geodynamic and exploration aspects. Mar. Pet. Geol., 18(4), 457–461.

Sørensen, A.B. (2006) Stratigraphy, structure and petroleum potential of the Lady Franklin and Maniitsoq Basins, offshore southern West Greenland. Petrol. Geosci., 12(3), 221–234.

Srivastava, S.P. (1978) Evolution of the Labrador Sea and its bearing on the early evolution of the North Atlantic. Geophys. J. Int., 52(2), 313–357.

St-Onge, M.R., Van Gool, J.A.M., Garde, A.A. & Scott, D.J. (2009) Correlation of Archaean and Palaeoproterozoic units between northeastern Canada and western Greenland: constraining the pre-collisional upper plate accretionary history of the Trans-Hudson orogen. Geol. Soc. London Spec. Publ., 318(1), 193–235.

Storey, M., Duncan, R.A., Pedersen, A.K., Larsen, L.M. & Larsen, H.C. (1998) 40Ar/39Ar geochronology of the West Greenland Tertiary volcanic province. Earth Planet. Sci. Lett., 160(3–4), 569–586.

Suckro, S.K., Gohl, K., Funck, T., Heyde, I., Ehrhardt, A., Schreckenberger, B., Gerlings, J., Damm, V. & Jokat, W. (2012) The crustal structure of southern Baffin Bay: implications from a seismic refraction experiment. Geophys. J. Int., 190(1), 37–58.

Suckro, S.K., Gohl, K., Funck, T., Heyde, I., Schreckenberger, B., Gerlings, J. & Damm, V. (2013) The Davis Strait crust-a transform margin between two oceanic basins. Geophys. J. Int., 193(1), 78–97.

Tappe, S., Foley, S.F., Stracke, A., Romer, R.L., Kjarsgaard, B.A., Heaman, L.M. & Joyce, N. (2007) Craton reactivation on the Labrador Sea margins: 40Ar/39Ar age and Sr-Nd-Hf-Pb isotope constraints from alkaline and carbonatite intrusives. Earth Planet. Sci. Lett., 256(3–4), 433–454.

Theunissen, K., Klerkx, J., Melnikov, A. & Mruma, A.H. (1996) Mechanisms of inheritance of rift faulting in the western branch of the East African Rift, Tanzania. Tectonics, 15(4), 776–790.

Thomas, W.A., Ravelo, A.C., Dekens, P.S. & McCarthy, M.D. (2006) Tectonic inheritance at a continental margin. GSA Today, 16(3), 4–11.

Umpleby, D.C. (1979) Geology of the Labrador shelf. Geol. Survey Canada, 79–13.

Van Gool, J.A.M., Connelly, J.N., Marker, M. & Mengel, F.C. (2002) The Nagssugtoqidian Orogen of West Greenland: tectonic evolution and regional correlations from a West Greenland perspective. Can. J. Earth Sci., 39(5), 665–686.

Wilson, T. (1966) Did the Atlantic close and the re-open? Nature, 209, 1246–1248.

Wilson, R.W., Klint, K.E.S., Van Gool, J.A.M., McCaffrey, K.J.W., Holdsworth, R.E. & Chalmers, J.A. (2006) Faults and fractures in central West Greenland: onshore expression of continental break-up and sea-floor spreading in the Labrador–Baffin Bay Sea. Geol. Survey Denmark Greenland Bulletin, 11, 185–204.

Wu, L., Trudgill, B.D. & Kluth, C.F. (2016) Salt diapir reactivation and normal faulting in an oblique extensional system, Vulcan Sub-basin, NW Australia. J. Geol. Soc., 173, https://doi.org/10.1144/jgs2016-008.

Figures

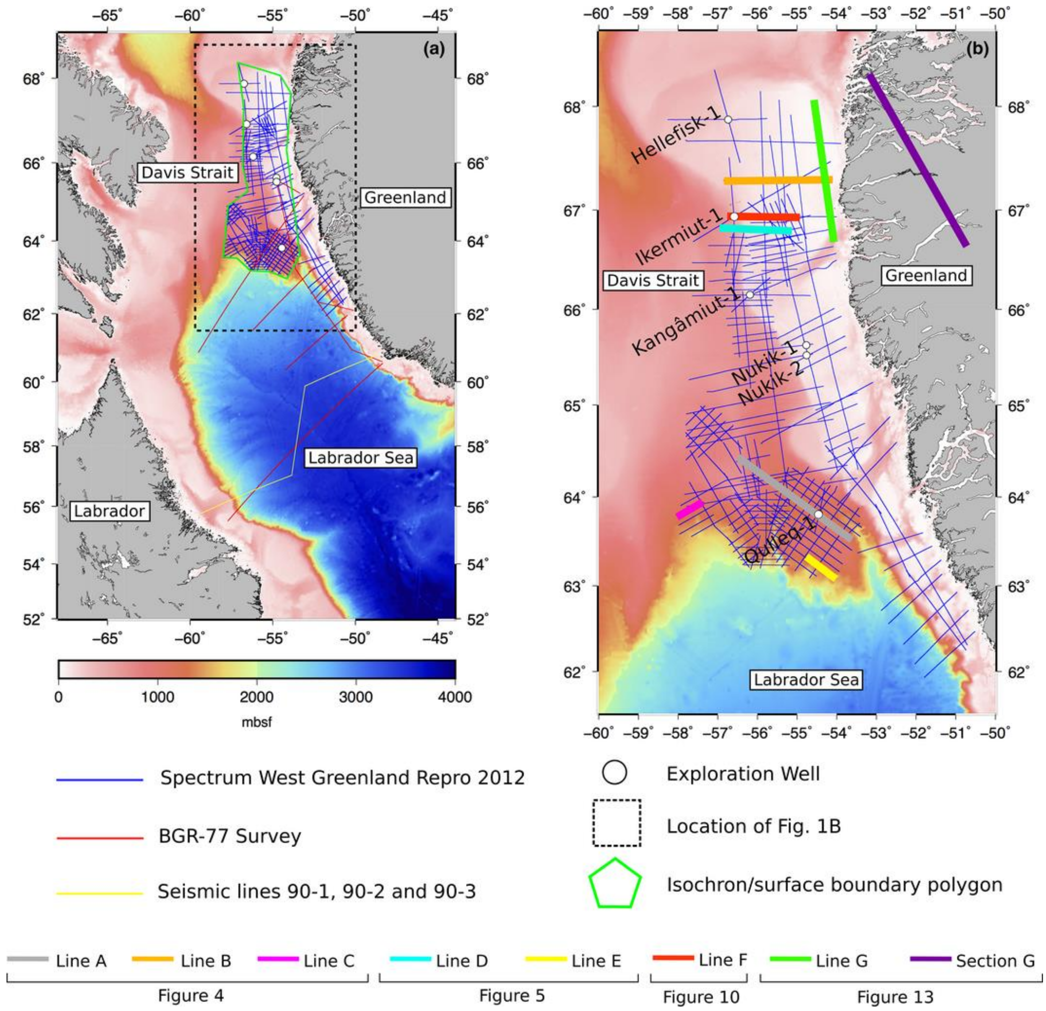

Figure 1. (a) The study area to the north of the Labrador Sea including: the locations of the seismic datasets, the polygon used for surface and isochron generation and the locations of the six exploration wells. (b) The study area within the eastern Davis Strait including the names of the six exploration wells in addition to the approximate locations of the seismic lines and geological cross section displayed in this contribution. Both (a) and (b) are plotted using the bathymetry data from Smith and Sandwell v17.1.

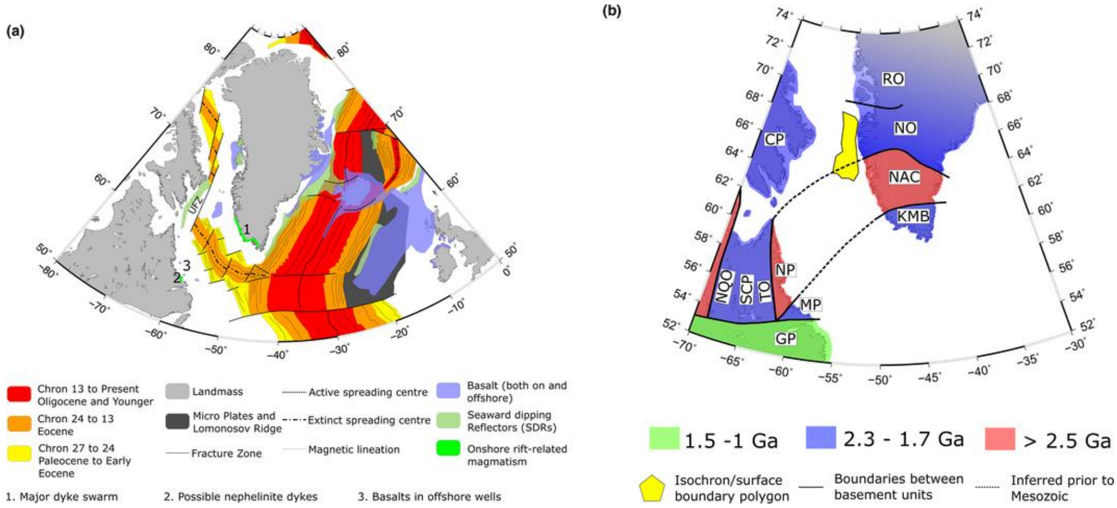

Figure 2. (a) An overview of the North Atlantic oceanic spreading systems, including: the age of oceanic crust; major active and extinct spreading axes; major oceanic fracture zones; proposed microplates and magnetic lineations (Oakey & Chalmers, 2012). The spatial distribution of onshore and offshore flood basalts and seaward dipping reflectors (SDRs) are overlain (Larsen & Saunders, 1998) in addition to the magmatism in the Labrador sea-Baffin Bay rift system described in previous work (Umpleby, 1979; Tappe *et al*., 2007; Larsen *et al*., 2009; Peace *et al*., 2016). (b) The primary study area (yellow polygon) within a simplified overview of basement units in north-eastern Canada and Greenland modified from Kerr *et al*. (1997) and Van Gool *et al*. (2002). RO, Rinkian Orogen; NO, Nagssugtoqidian; CP, Churchill Province; NQO, New Quebec Orogen; SCP, Southern Churchill Province; TO, Torngat Orogen; NP, Nain Province; MP, Makkovik Province; GP, Grenville Province; NAC, North Atlantic Craton; KMB, Ketilidian Mobile Belt.

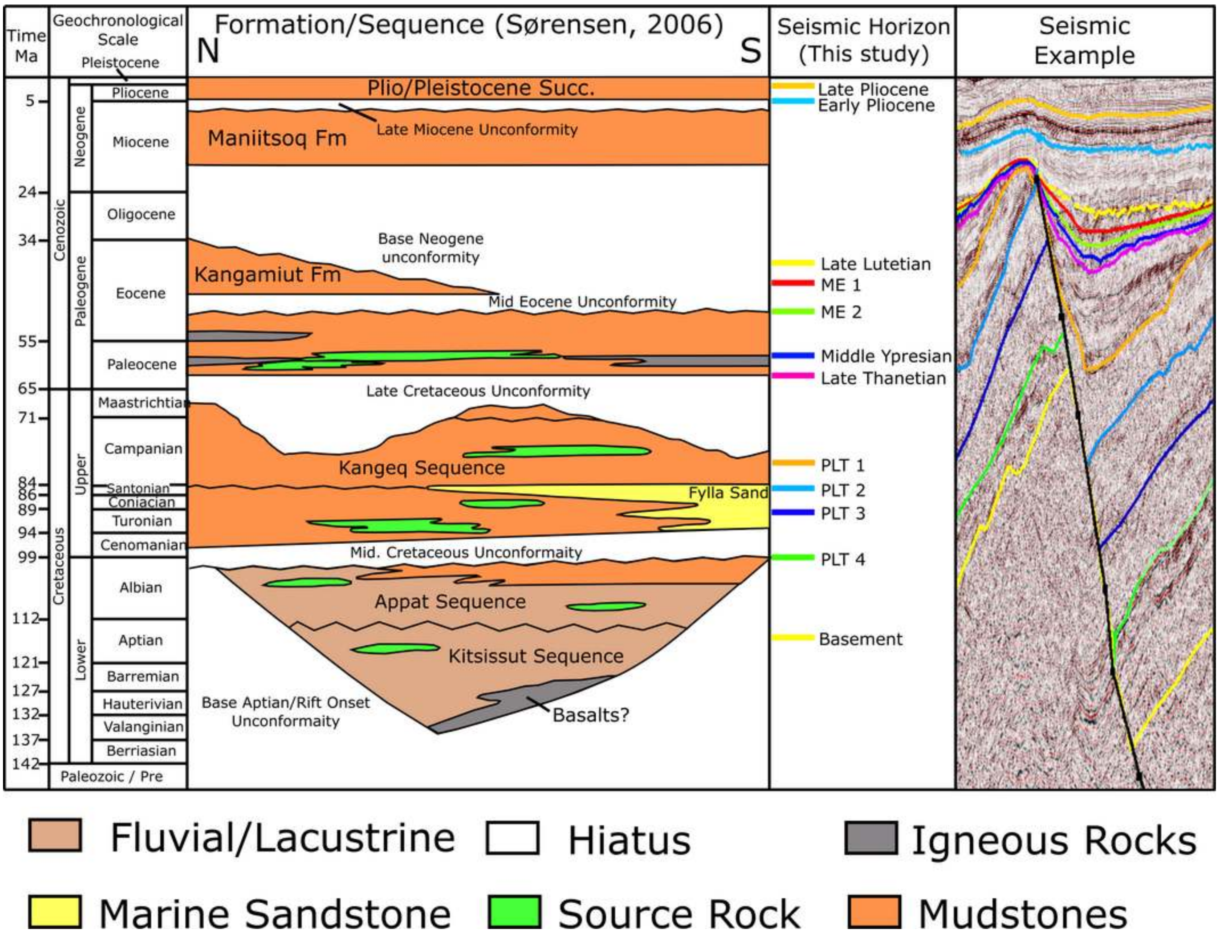

Figure 3. Stratigraphic framework for the study area (Fig. 1) modified from Sørensen (2006) to include the stratigraphic locations of the horizons interpreted in this study and an example seismic section.

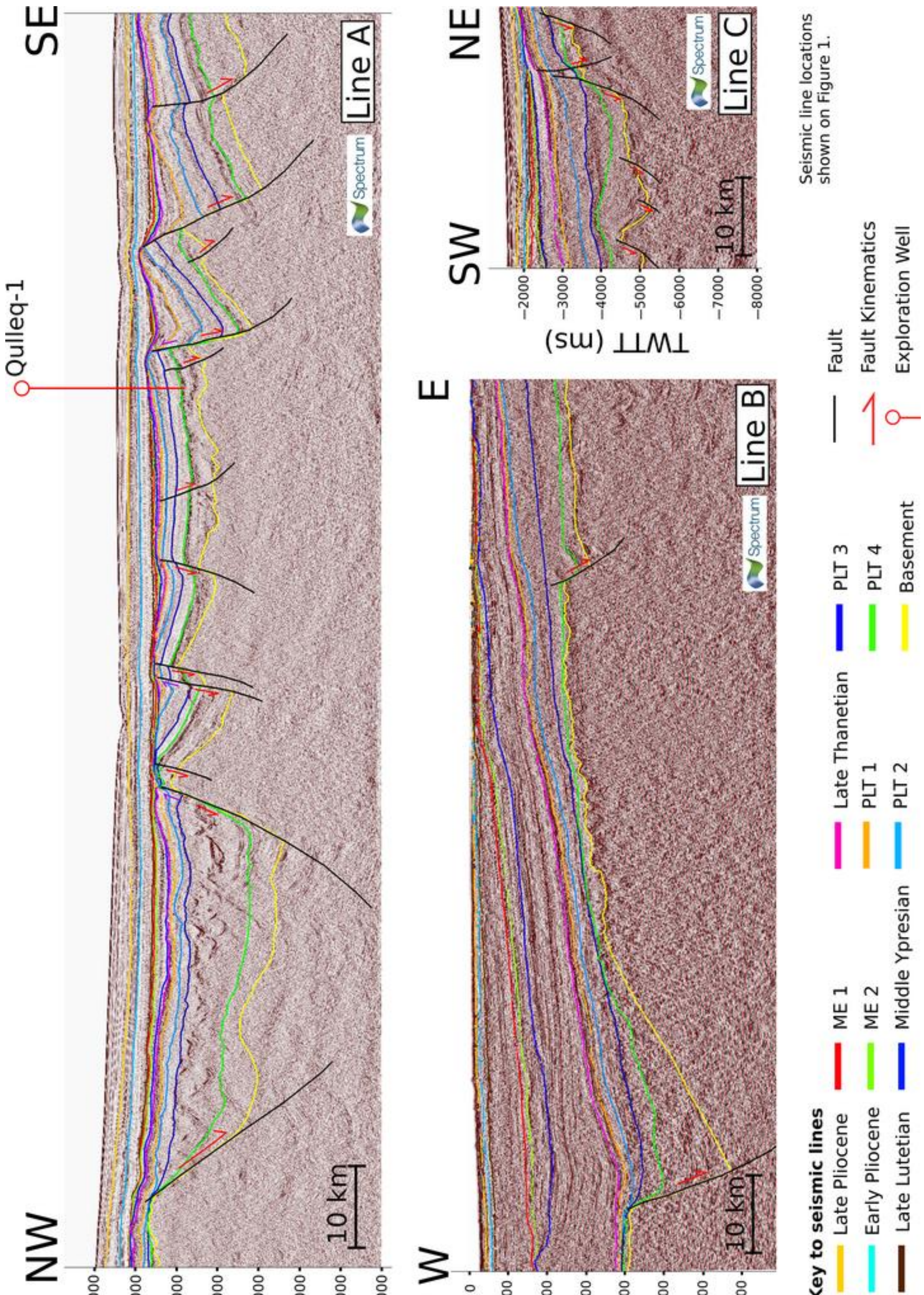

Figure 4. Representative seismic reflection profiles from across the study area (Fig. 1b). Line A is a NW-SE oriented seismic line from the southeast of the study area, Line B is a W-E trending seismic line from the north of the study area and Line C is a NE-SW trending seismic line from the southwest of the study area.

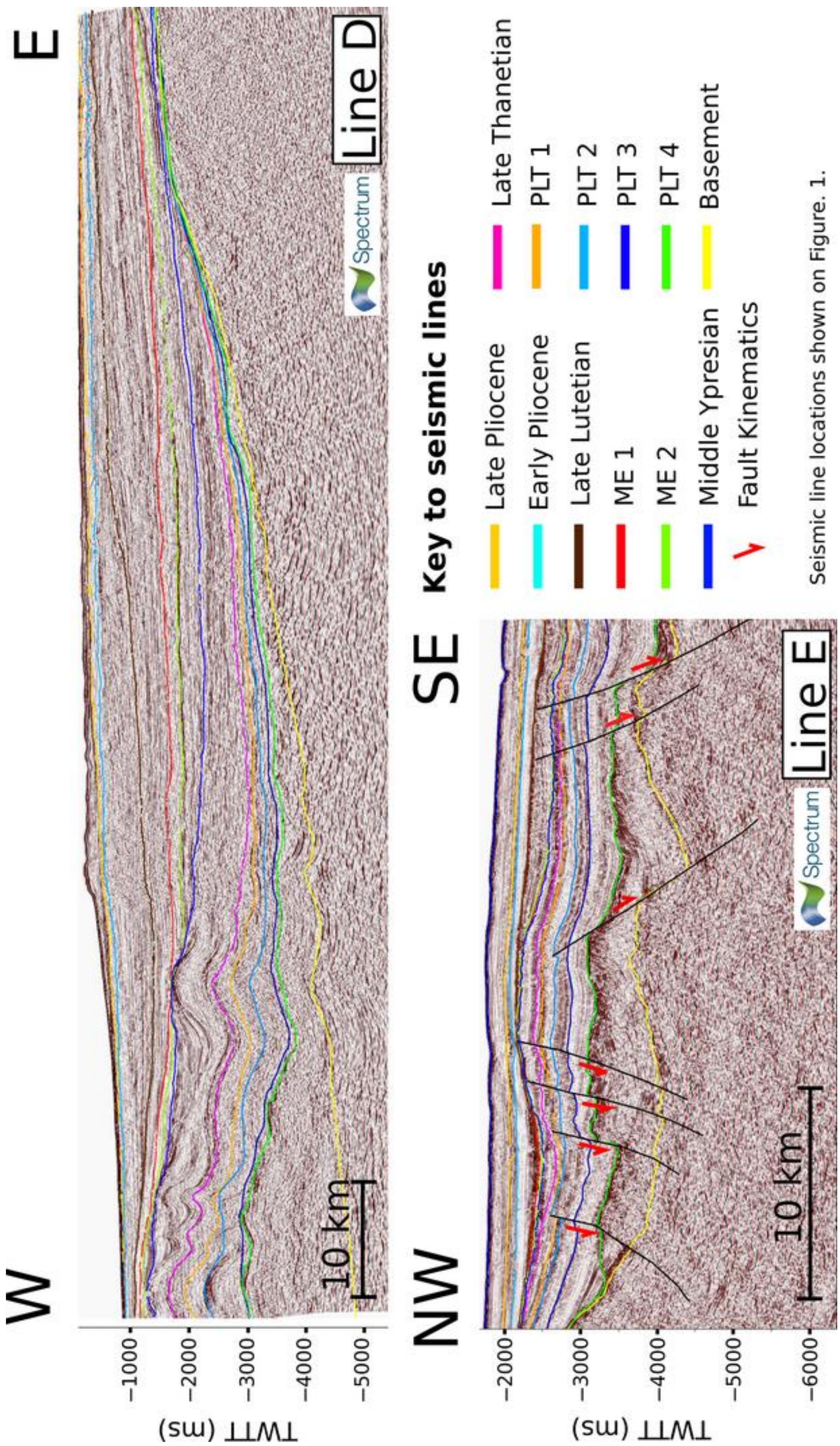

Figure 5. Line D is a W-E trending seismic line from the north of the study area and Line E is a NW-SE oriented seismic line from the south of the study area.

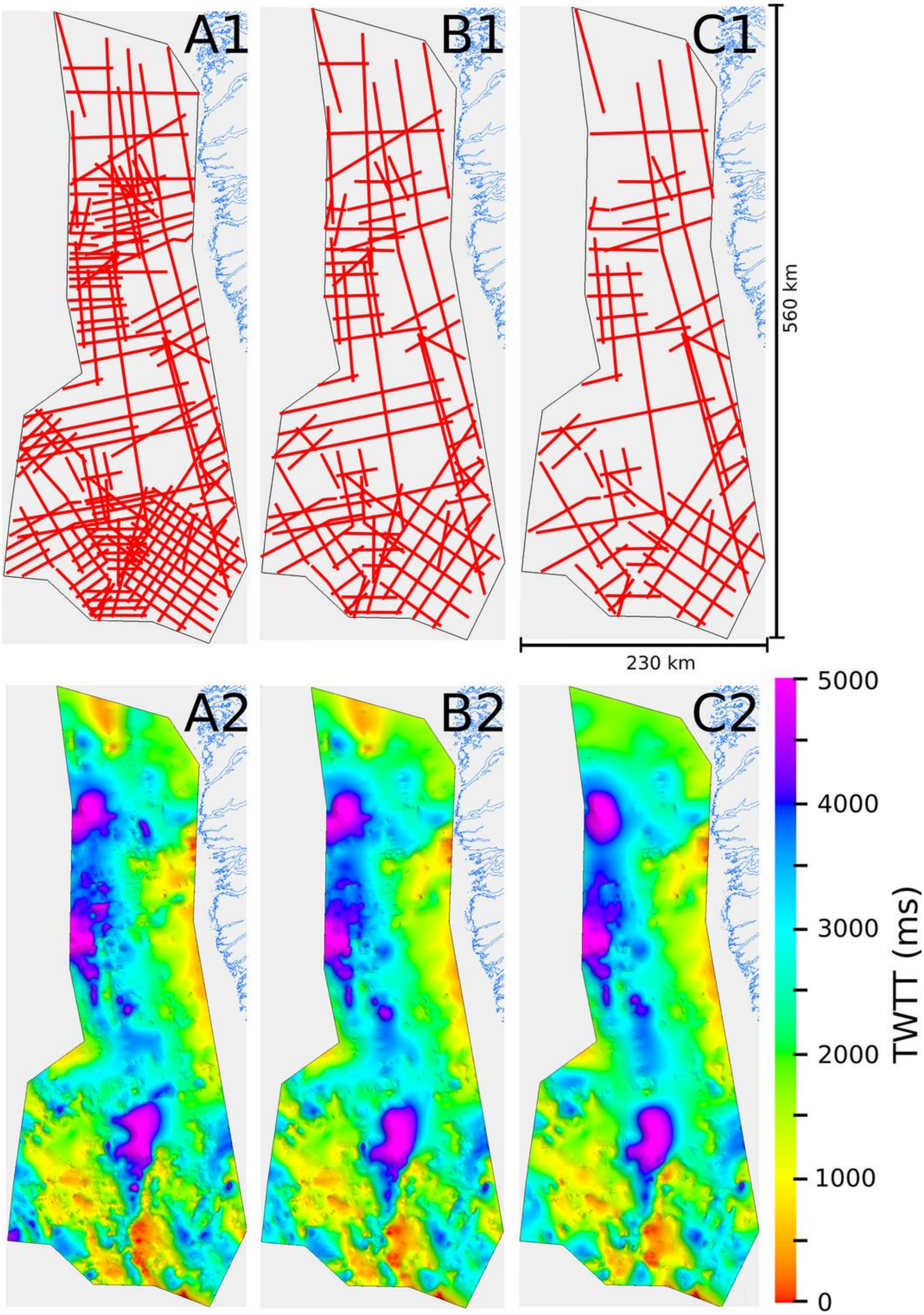

Figure 6. Total sediment thickness (top basement horizon to seabed) maps produced after thinning the seismic grid. The seismic grid above each isochron depicts the lines used to produce the isochron below.

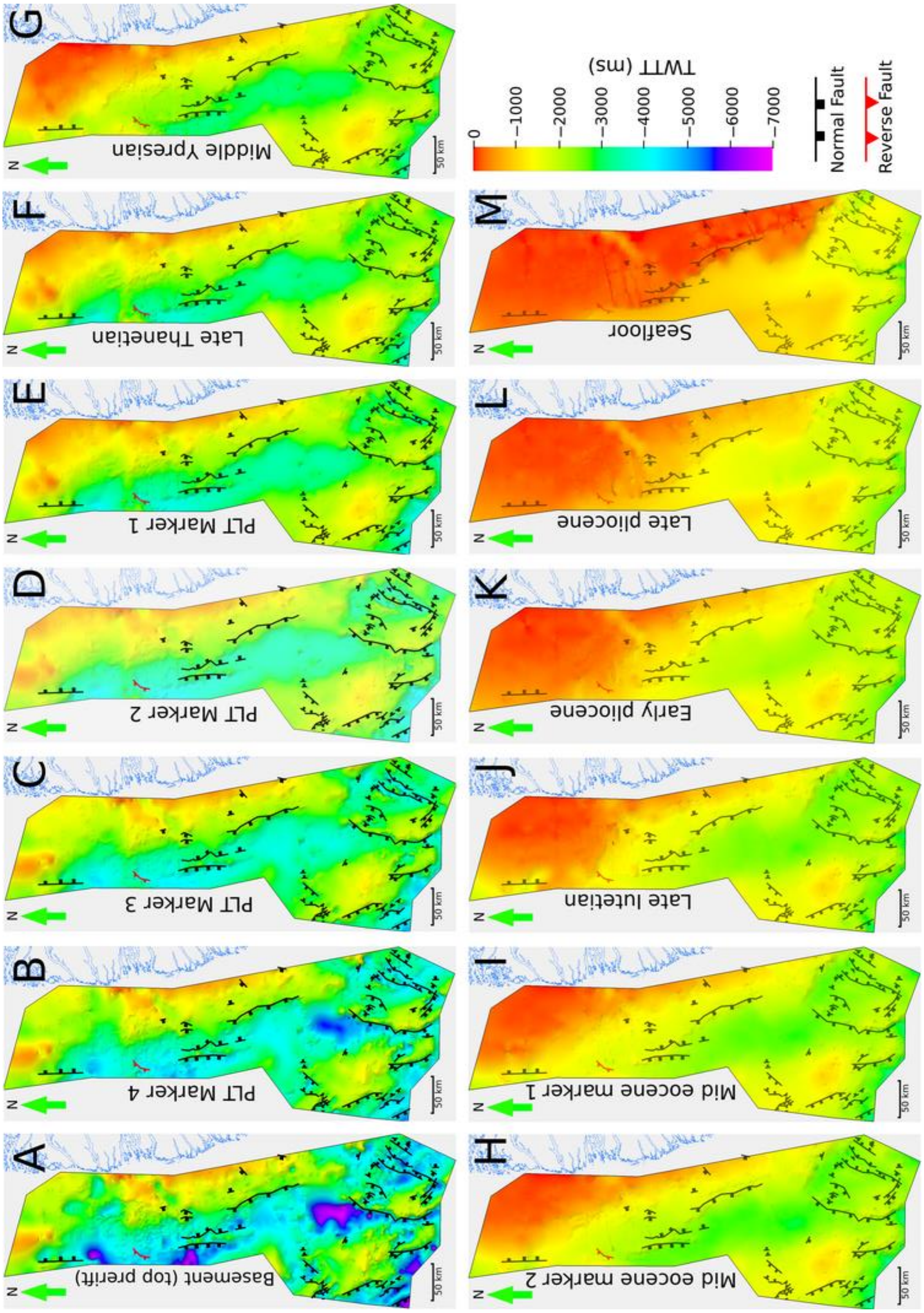

Figure 7. Surfaces generated from each interpreted horizon, along with the interpreted faults with transparency increasing through time to indicate the diminishing role of such structures. PLT, Pre-Late Thanetian.

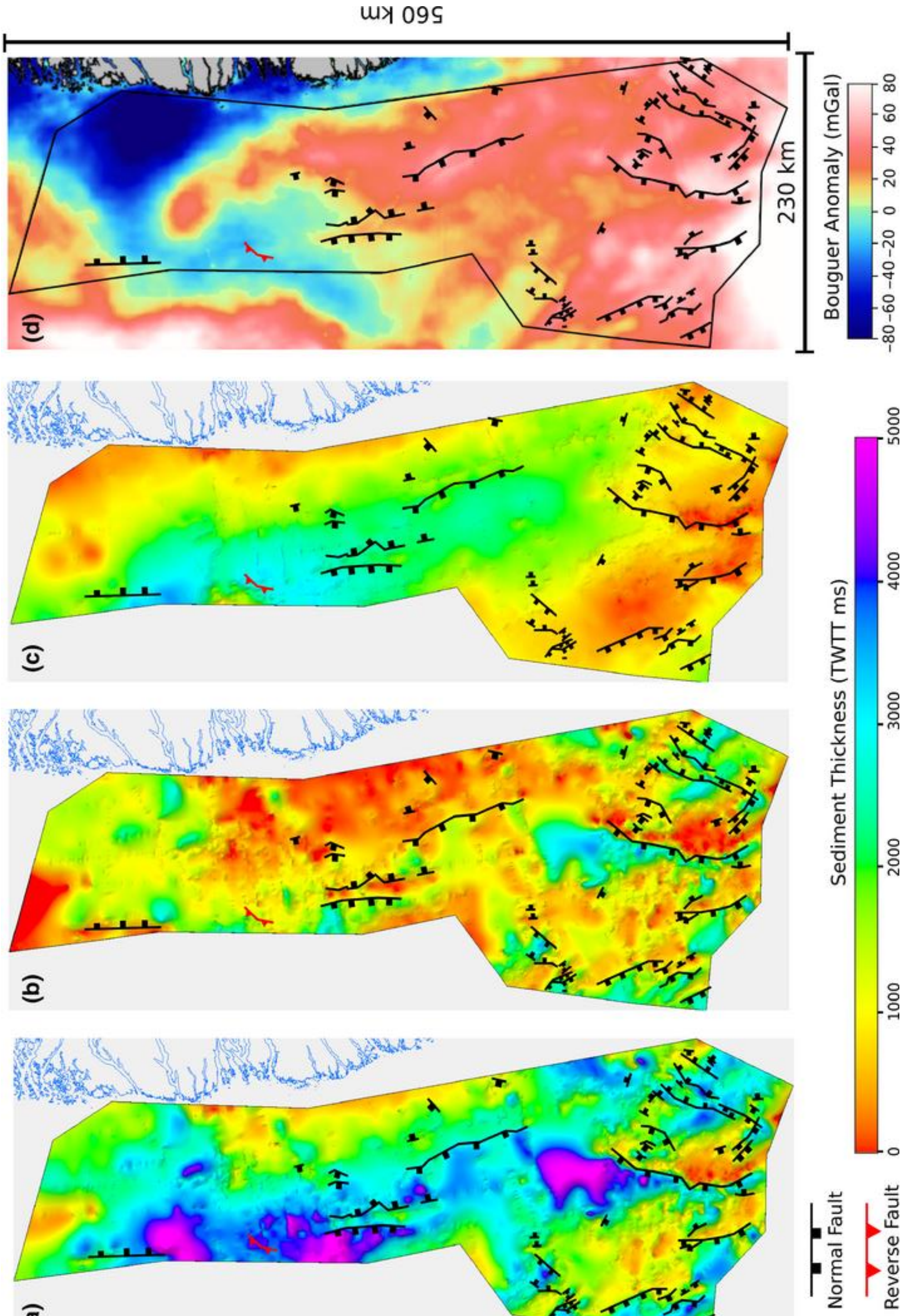

Figure 8. Time thickness isochrons for: (a) Total sediment thickness, (b) Basement to Late Thanetian and (c) Late Thanetian to Seafloor (all in TWTT ms). (d) The Bouguer gravity anomaly calculated using Smith and Sandwell free air anomaly v23.1 by assuming an average crustal density of 2.7 g cm^{-3}. Also shown are the faults interpreted during this study.

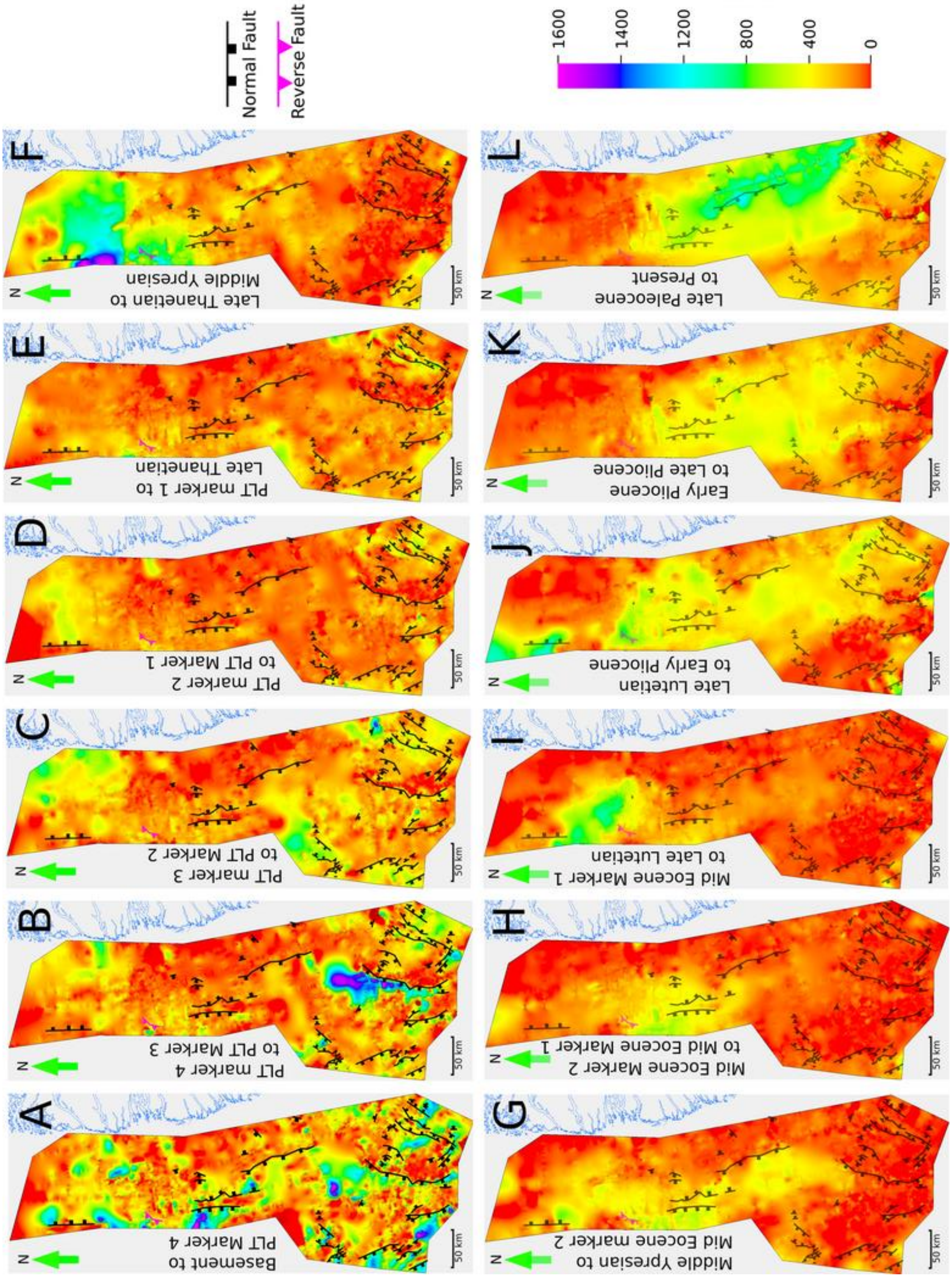

Figure 9. Isochrons for the defined geological intervals used in this study. Also shown are the interpreted faults with transparency increasing through time to indicate the diminishing role of such structures.

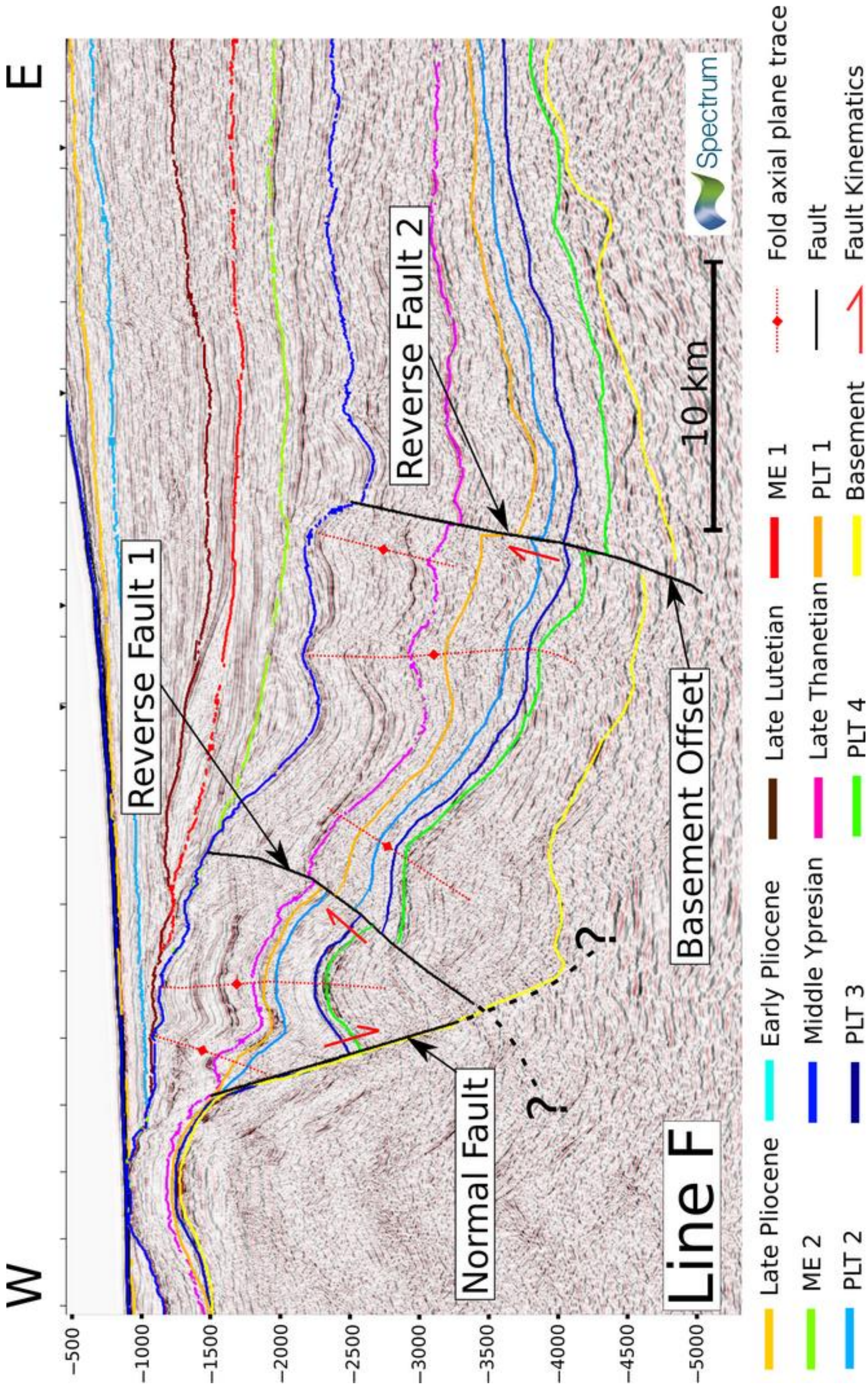

Figure 10. Seismic reflection Line F (location shown on Fig. 1b) through part of the Ikermiut Fault Zone and associated folding predating the Middle Ypresian horizon.

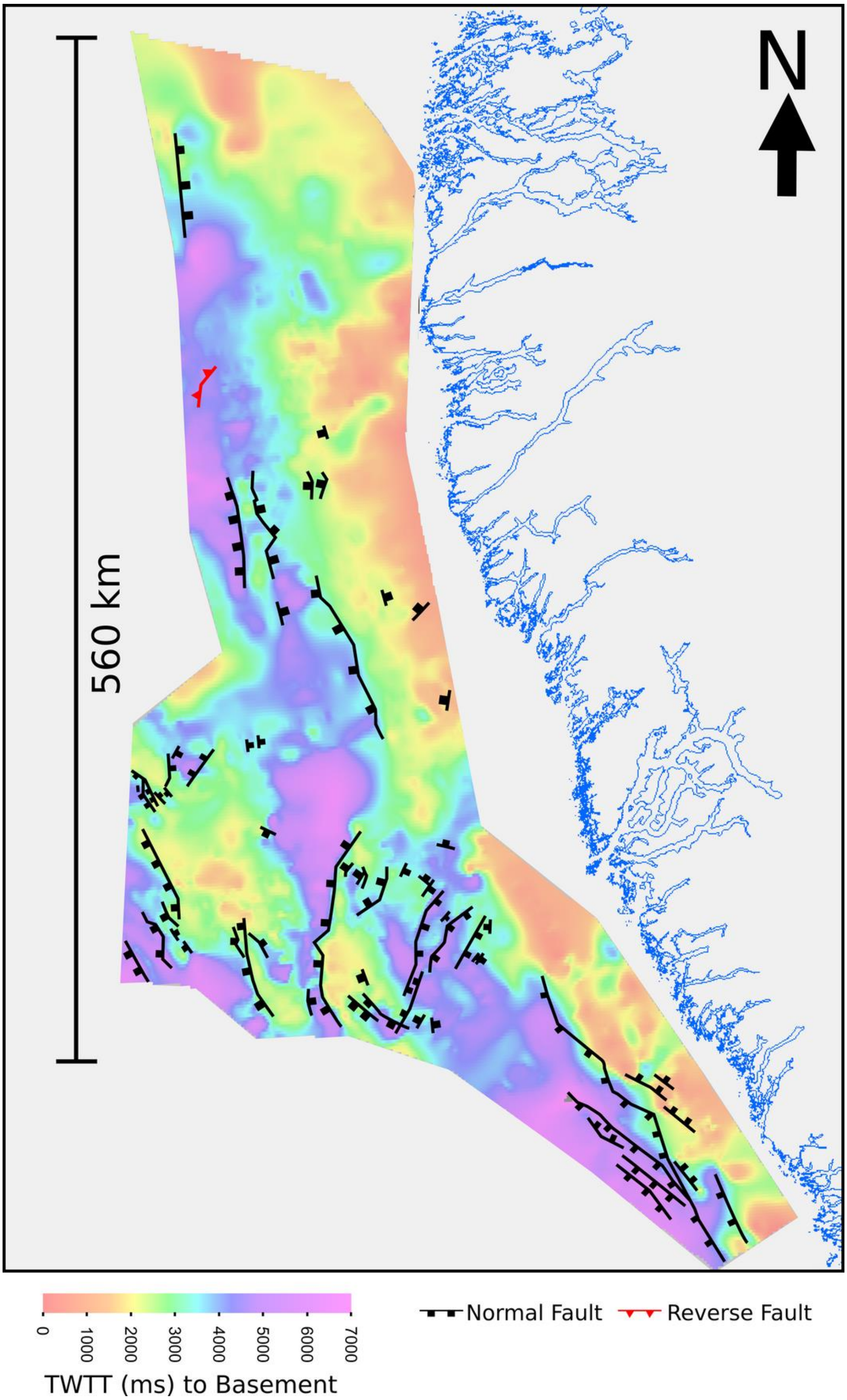

1116 Figure 11. Offshore fault map for the Eastern Davis Strait produced by this study
1117 overlain on the basement horizon in TWTT (ms).
1118

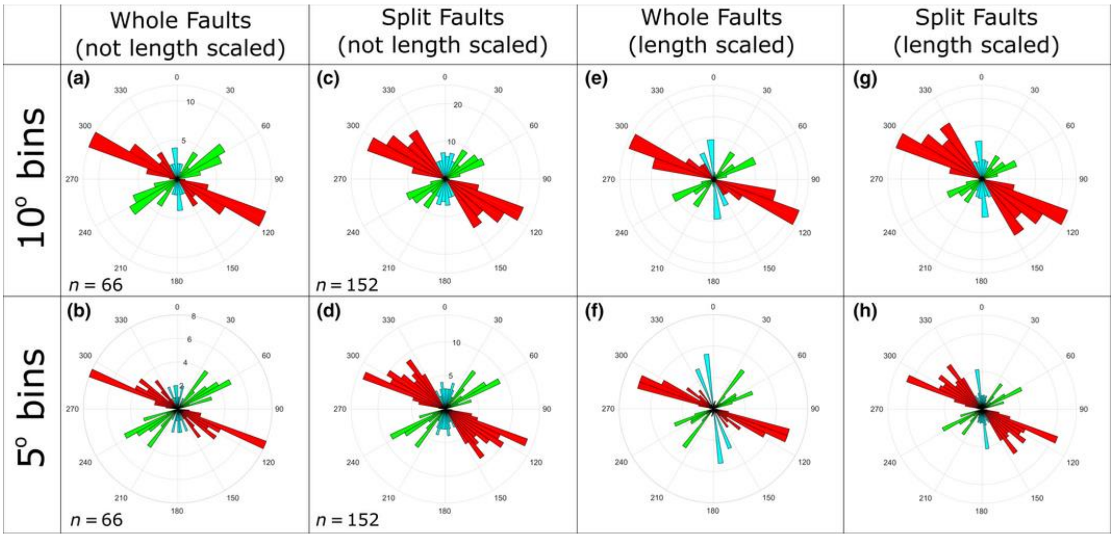

Figure 12. (a) Rose diagram for whole faults with 10° bins and not length scaled. (b) Rose diagram for whole faults with 5° bins and not length scaled. (c) Rose diagram for faults split at vertices with 10° bins and not length scaled. (d) Rose diagram for faults split at vertices 5° bins and not length scaled. (e) Rose diagram for whole faults with 10° bins and length scaled. (f) Rose diagram for whole faults with 5° bins and length scaled. (g) Rose diagram for faults split at vertices with 10° bins and length scaled. (h) Rose diagram for faults split at vertices 5° bins and length scaled.

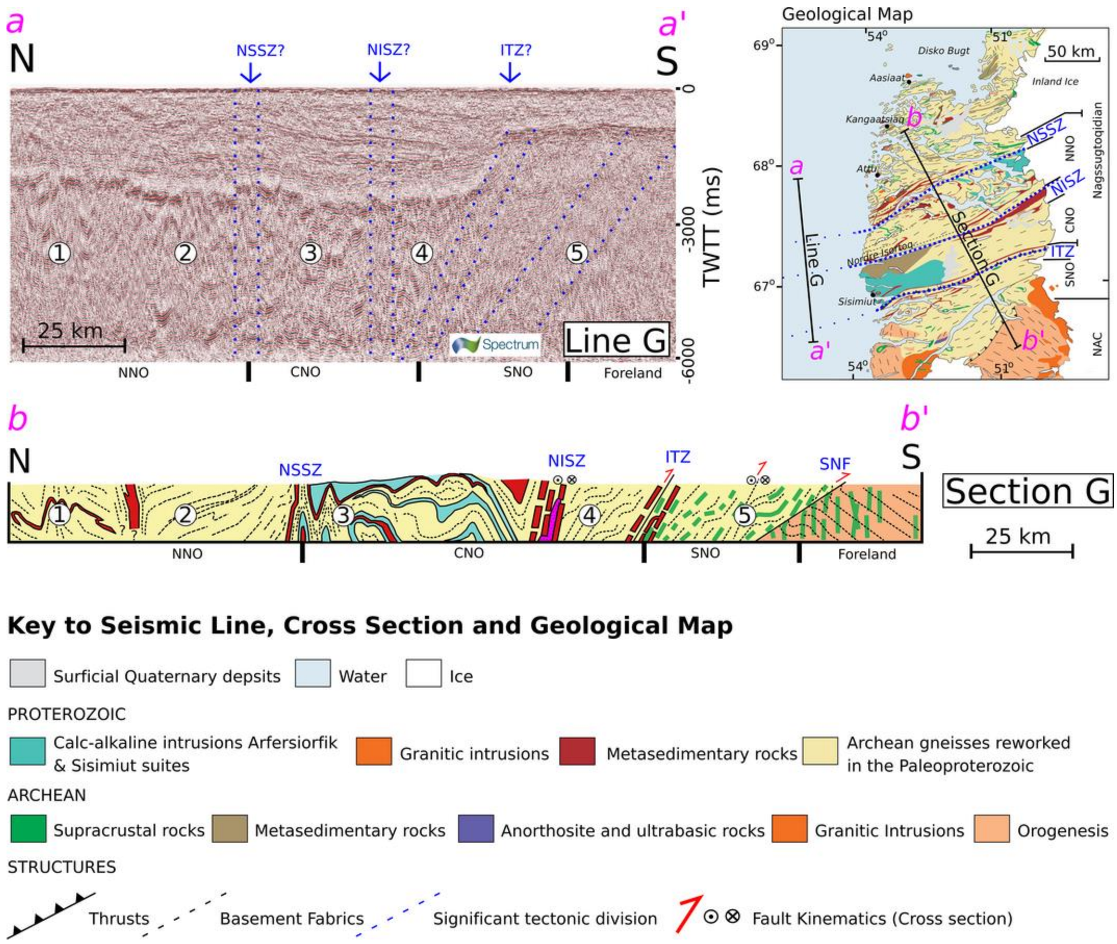

Figure 13. Line G (a–a′) is a N-S oriented seismic line from the northeast of the study area that lies approximately adjacent to the onshore geological cross section G (b–b′), as shown on the geological map insert on this figure. The geological map and cross section of the Nagssugtoqidian orogen are modified from Van Gool *et al*. (2002) and Wilson *et al*. (2006). NSSZ, Nordre Strømfjord shear zone; NISZ, Nordre Isortoq shear zone; ITZ, Ikertôq thrust zone; NNO, Northern Nagssugtoqidian orogeny; CNO, Central Nagssugtoqidian orogeny; SNO, Southern Nagssugtoqidian orogeny; SNF, Southern Nagssugtoqidian front; NAC, North Atlantic Craton.

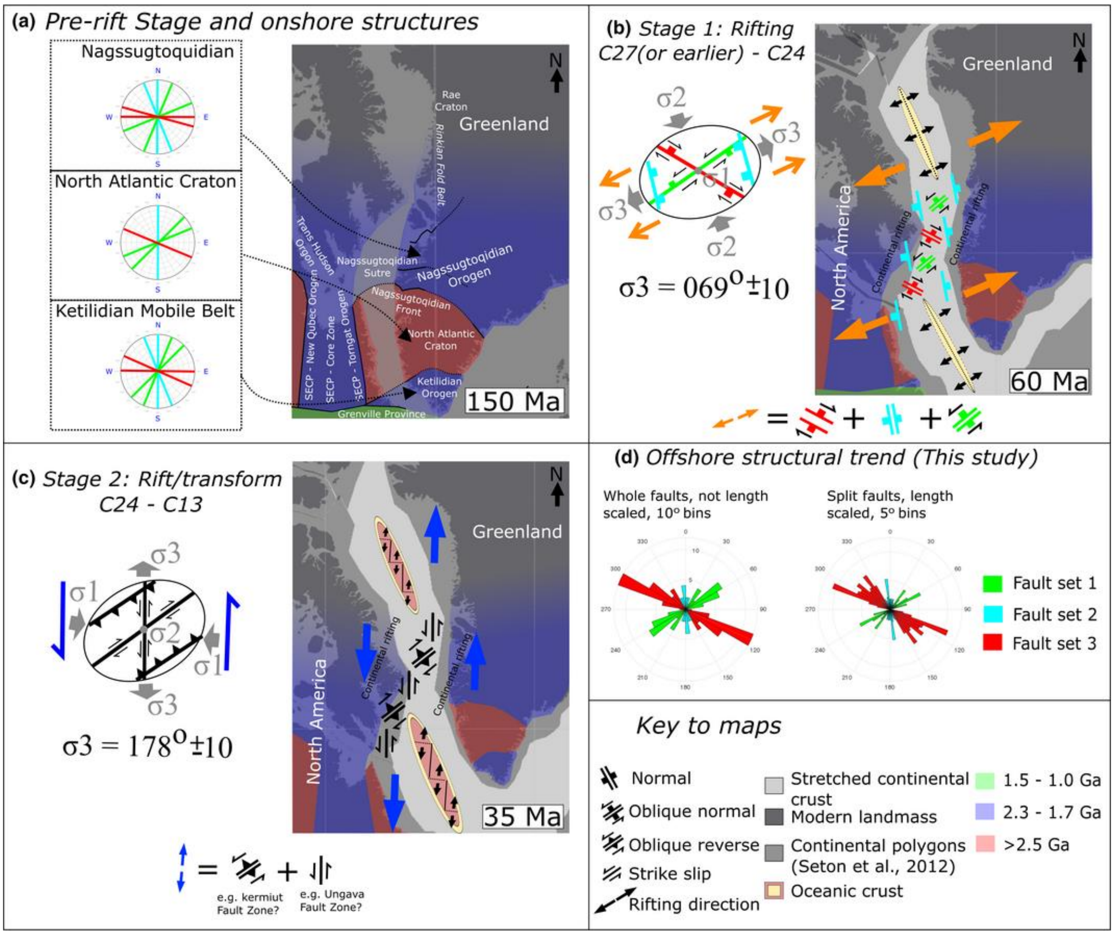

Figure 14. (a) The pre-rift configuration of North America and Greenland along with graphical representations of the onshore structures in the basement terrains of West Greenland (Japsen *et al*., 2006; Wilson *et al*., 2006) coloured using the same colours for similar orientation structure sets as in this study (Fig. 12). (b) Kinematic model for the first rifting stage. (c) Kinematic model for the second rifting stage where the Ungava Transform Fault system develops as a result of the lateral offset between Baffin Bay and the Labrador Sea (possibly due to the Nagssugtoqidian and Torngat orogens) and the newly established N-S rifting direction in this interval. (d) Summary of the offshore faults as characterized in this study. (e) Key to the maps in parts (a), (b) and (c) of this figure.

Tables

Well Name	Latitude	Longitude	Date	TD (m)	TD Lithology/Formation
Hellefisk-1	67.877944	-56.739161	21/06/1977	3201.2	Basalt (Paleocene?)
Ikermiut-1	66.936572	-56.590681	12/07/1977	3619	Campanian shales
Kangamiut-1	66.150256	-56.190078	02/06/1976	3874	Precambrian basement
Nukik-1	65.526719	-54.760497	02/07/1977	2363.4	Precambrian basement
Nukik-2	65.631775	-54.766831	08/08/1977	2693.8	Masstrichtian Basalt
Qulleq-1	63.813342	-54.451836	10/07/2000	2973	Santonian Sandstones

Table 1. Summary of exploration wells used in this study in the Davis Strait with the terminal depth (TD) in metres from the rotary table. Lithology at TD from Nøhr-Hansen (2003) and Rolle (1985).

System No.	Ketilidian Mobile Belt (Japsen *et al.* 2006)			North Atlantic Craton (Japsen *et al.* 2006)				Nagssugtoqidian (Wilson *et al.* 2006)	This Study
	Landsat		Field	Landsat		Aerial	Field	Landsat, Aerial, Field	Seismic interpretation
	1:500,000	1:100,000		1:500,000	1:100,000				
1	NE-SW	No Dominant system. A range from NE-SW through to SE-NW.	N-S	N-S	N-S		N-S	ENE-WSW	NE-SW
2	N-S		NE-SW/ENE-WSW	NE-SW	NE-SW	NE-SW	NE-SW	N-S	NNW-SSE
3	NNW-SSE		E-W	ENE-WSW	ENE-WSW	ENE-WSW	ENE-WSW	NNW-SSE	NW-SE
4	NNE-SSW		ESE-WNW/ SE-NW	ESE-WNW	ESE-WNW		NW-SE	NNE-SSW	
5	E-W to ESE-WNW							E-W to ESE-WNW	

Table 2. Summary of the onshore structural systems identified using different methodologies in the Ketilidian Mobile Belt, the North Atlantic Craton (Japsen *et al.*, 2006) and the Nagssugtoqidian by Wilson *et al.* (2006) and Japsen *et al.* (2006). Orientations quoted in this table represent the strike of the feature.